




# Resistive gas sensors based on metal-oxide nanowires F

Cite as: J. Appl. Phys. **126**, 241102 (2019); <https://doi.org/10.1063/1.5118805>

Submitted: 09 July 2019 . Accepted: 04 December 2019 . Published Online: 23 December 2019

 Ali Mirzaei, Jae-Hyoung Lee,  Sanjit Manohar Majhi, Matthieu Weber,  Mikhael Bechelany, Hyoun Woo Kim, and  Sang Sub Kim

## COLLECTIONS

F This paper was selected as Featured



View Online



Export Citation



CrossMark

## ARTICLES YOU MAY BE INTERESTED IN

### Gas sensing in 2D materials

Applied Physics Reviews **4**, 021304 (2017); <https://doi.org/10.1063/1.4983310>

### Functional gas sensing nanomaterials: A panoramic view

Applied Physics Reviews **7**, 021301 (2020); <https://doi.org/10.1063/1.5123479>

### Engineering of defects in resistive random access memory devices

Journal of Applied Physics **127**, 051101 (2020); <https://doi.org/10.1063/1.5136264>



Webinar  
How to Characterize Magnetic  
Materials Using Lock-in Amplifiers

Zurich Instruments MFLI

Zurich Instruments

CRYOGENIC

Register now

# Resistive gas sensors based on metal-oxide nanowires

Cite as: J. Appl. Phys. **126**, 241102 (2019); doi: [10.1063/1.5118805](https://doi.org/10.1063/1.5118805)

Submitted: 9 July 2019 · Accepted: 4 December 2019 ·

Published Online: 23 December 2019



Ali Mirzaei,<sup>1,a)</sup>  Jae-Hyoung Lee,<sup>2</sup> Sanjit Manohar Majhi,<sup>2,3,4</sup>  Matthieu Weber,<sup>5</sup> Mikhael Bechelany,<sup>5,a)</sup>   
Hyouon Woo Kim,<sup>3,4,a)</sup> and Sang Sub Kim<sup>2,a)</sup> 

## AFFILIATIONS

<sup>1</sup>Department of Materials Science and Engineering, Shiraz University of Technology, Shiraz 715557-13876, Iran

<sup>2</sup>Department of Materials Science and Engineering, Inha University, Incheon 22212, South Korea

<sup>3</sup>The Research Institute of Industrial Science, Hanyang University, Seoul 04763, South Korea

<sup>4</sup>Division of Materials Science and Engineering, Hanyang University, Seoul 133-791, South Korea

<sup>5</sup>Institut Européen des Membranes (IEM)–UMR 5635, ENSCM, CNRS, University of Montpellier, Place Eugène Bataillon, 34095 Montpellier cedex 5, France

**a) Authors to whom correspondence should be addressed:** [alimirzaei@sutech.ac.ir](mailto:alimirzaei@sutech.ac.ir); [mikhael.bechelany@umontpellier.fr](mailto:mikhael.bechelany@umontpellier.fr);  
[hyouonwoo@hanyang.ac.kr](mailto:hyouonwoo@hanyang.ac.kr); and [sangsub@inha.ac.kr](mailto:sangsub@inha.ac.kr)

## ABSTRACT

Gas sensors are indispensable for detecting harmful gases in the environment. The morphology of a gas sensor significantly affects its sensing performance. Among the various morphologies, one-dimensional nanowires (NWs) have numerous advantages, such as high surface area, small dimensions, high charge-carrier concentrations, facile synthesis, high crystallinity, and stability. These excellent properties make NWs promising for gas sensing. Resistive-type metal oxide-based gas sensors are widely used for monitoring various toxic gases and volatile organic compounds. In this tutorial, the synthesis of metal oxide NWs, the fabrication of gas sensors, and their sensing mechanisms are discussed. Different types of NW-based gas sensors, such as single NWs, branched NWs, noble metal-functionalized NWs, heterojunction NWs, self-heating NWs, ultraviolet-activated NWs, core-shell NWs, and electronic-nose-based NWs, are comprehensively presented. Finally, we discuss future directions with regard to the improvement and potential of these NW gas sensors. This tutorial aims to provide an overview of the fundamental principle and state-of-the-art technology, which is useful for researchers and students working in the field of resistive-type NW-based gas sensors.

Published under license by AIP Publishing. <https://doi.org/10.1063/1.5118805>

## I. TOXIC GASES AND VAPORS

Gases are intimately linked to life, as most living species continuously need to breathe air, which is a mixture of O<sub>2</sub>, N<sub>2</sub>, Ar, and other gases. Additionally, many gases are used in industry and for domestic purposes. For example, liquefied petroleum gas (LPG) is widely used for cooking and heating, as well as in many industrial areas.<sup>1</sup> Although LPG is nontoxic, it is highly explosive.<sup>2</sup> H<sub>2</sub> gas is regarded as the next “green fuel” and is currently used in fuel cells, although it is highly explosive.<sup>3,4</sup> In addition to explosive gases, the number of toxic and hazardous gases has significantly increased in recent years due to the increase in automobiles and rapid industrialization, causing severe indoor and outdoor pollution and many adverse health effects.<sup>5</sup> Toxic gases can cause harm at low concentrations

over long periods of time (chronic exposure) or at higher concentrations over short periods of time (acute exposure). The threshold limit value (TLV) is defined as the maximum concentration of a gas that is allowed during a working day of 8 h for repeated exposure without resulting in adverse health effects.<sup>6</sup> For example, the TLVs for carbon monoxide (CO), nitrogen dioxide (NO<sub>2</sub>), and hydrogen sulfide (H<sub>2</sub>S) gases are 50, 3, and 10 ppm, respectively.<sup>6</sup>

According to the World Health Organization, air pollution is mainly caused by toxic gases and led to approximately  $7 \times 10^6$  premature deaths in 2012.<sup>7</sup> Many toxic gases exist in the atmosphere; for example, carbon monoxide (CO), a major air pollutant that results from the burning of fossil fuels, car exhaust, and emissions from industrial factories.<sup>8,9</sup> CO poisoning results in >5000 deaths

per year in the USA.<sup>10</sup> In Denmark, from 1995 to 2015, there were several hundred fatalities due to CO poisoning.<sup>11</sup> Additionally, in Iran, a developing country, approximately 836 deaths occurred in 2016 due to CO poisoning.<sup>12</sup> CO is a tasteless, colorless, and odorless gas that has 240 times greater affinity for hemoglobin compared with O<sub>2</sub>.<sup>13</sup> It forms carboxyhemoglobin, which leads to reduced O<sub>2</sub> delivery to tissues and can cause tissue hypoxia.<sup>6,10,14</sup> Additionally, CO easily binds to cytochrome oxidase and leads to lactic acidosis, apoptosis, and hypoxia.<sup>14</sup> Another example of a hazardous gas is nitrogen dioxide (NO<sub>2</sub>), which is known as an oxidizing gas.<sup>15</sup> Long-term exposure to NO<sub>2</sub> can result in inflammation of lung tissue, silo-filler's disease, and bronchiolitis fibrosis obliterans. Additionally, NO<sub>2</sub> released by jets in the atmosphere can damage the ozone layer.<sup>16</sup> Hydrogen sulfide (H<sub>2</sub>S) is another highly poisonous gas and can be produced from the bacterial decomposition of organic materials. Moreover, H<sub>2</sub>S is a by-product of many industries, including waste management, petroleum refining, and natural-gas production.<sup>17</sup> At low concentrations (50 ppm), it can cause problems to the eyes and the respiratory system. However, at a concentration of 100 ppm, H<sub>2</sub>S gas can paralyze the olfactory nerves and disable the sense of odor. Long-term exposure to 250-ppm H<sub>2</sub>S causes asphyxia and may lead to suffocation. Exposure to 1000-ppm H<sub>2</sub>S paralyzes the respiratory nerve center and may cause sudden physical collapse.<sup>18</sup> Furthermore, high concentrations of H<sub>2</sub>S are associated with chronic bronchitis, emphysema, pneumonia, and cardiovascular diseases such as hypertension.<sup>19</sup>

Volatile organic compounds (VOCs)—organic chemicals with a high vapor pressure (101.325 kPa) and low boiling point—are another type of major air pollutant.<sup>20</sup> Common examples of VOCs are benzene, xylene, toluene (BTX), ethanol, acetone, formaldehyde, *n*-butanol, acetaldehyde, and methanol.<sup>6,21</sup> Most VOCs cause atmospheric pollution and are toxic to humans (carcinogenic, mutagenic, or teratogenic).<sup>22–24</sup> Accumulation of some VOCs can lead to building-related illnesses and the “sick building syndrome,” which is associated with headaches and nausea.<sup>25</sup> Details regarding the physical properties, exposure limit values, and adverse effects on human health for various toxic gases, VOCs, and combustible gases can be found in the article of Majhi *et al.*<sup>6</sup>

## II. GAS SENSORS: GENERAL OVERVIEW

Even though the human olfactory system has long been considered the least significant of the human senses,<sup>26</sup> it is highly important, as it warns us about potential air hazards. Additionally, it is the only active sense during sleep.<sup>27–29</sup> The human olfactory system can discriminate approximately 400 000 odors.<sup>30</sup> Additionally, the olfactory system of humans is more sensitive than those of rodents and dogs for some odors.<sup>31</sup> However, when the concentration of a gas is very low or the gas is odorless, it cannot be sensed by the human olfactory system. Therefore, sensitive technological devices are necessary to detect the presence of the toxic and dangerous gases in our environment. Traditionally, mass spectrometers,<sup>32</sup> gas chromatographs,<sup>33</sup> flame ionization detectors,<sup>34</sup> and Fourier transform infrared spectrometers<sup>35</sup> have been utilized for the detection and analysis of toxic gases. These analytical devices are usually bulky and expensive and often require trained operators. Therefore, they are used in laboratories for specific

purposes.<sup>36</sup> Furthermore, they cannot be used for onsite measurements due to their size, limiting their wide range of applications.

In contrast to bulky analytical instruments, gas sensors are typically small and do not need sample preparation.<sup>37</sup> The gas sensor is a subcategory of chemical sensors and can be defined as a device that transforms chemical information (e.g., concentrations of a specific gas) into an analytically useful signal (current, voltage, impedance/conductance, or frequency).<sup>38</sup> Various gas sensors have been developed and studied that are based on different working principles, such as surface acoustic wave gas sensors,<sup>39</sup> electrochemical gas sensors,<sup>40,41</sup> optical gas sensors,<sup>42,43</sup> gasochromic gas sensors,<sup>44,45</sup> quartz crystal microbalance gas sensors,<sup>46</sup> catalytic gas sensors,<sup>47,48</sup> thermal-conductivity gas sensors,<sup>49,50</sup> cataluminescence sensors,<sup>46,51</sup> and resistive-based gas sensors.<sup>52,53</sup> In this tutorial paper, the different aspects of resistive-based metal-oxide nanowire (NW) gas sensors whose operation is based on the resistance changes in the presence of the target gases are presented.

## III. METAL OXIDE-BASED GAS SENSORS: BRIEF HISTORY

The evaluation of the first gas sensor was realized in the early 1920s, when people used canaries for the detection of poisonous gases in mines. These birds were found to be more sensitive to methane, CO gas, and low O<sub>2</sub> concentrations than humans.<sup>54,55</sup> The use of semiconductors as gas sensors started in 1953, when Brattain and Bardeen found direct evidence for the existence of an electron-depletion region at the free surface of Ge (a semiconducting material).<sup>56</sup> Then, in 1954, Heiland found a correlation between the electrical resistance of ZnO and H<sub>2</sub> gas when ZnO was placed in a H<sub>2</sub> gas atmosphere.<sup>57</sup> In 1962, Seiyama *et al.* used ZnO as a gas sensor for the detection of toluene, benzene, carbon dioxide, propane, ethyl ether, and ethyl alcohol gases.<sup>58</sup> This was the first device that utilized the resistance changes in a metal-oxide semiconductor resulting from gas adsorption. In Japan, a great catastrophe occurred in 1962 due to the explosion accidents of supplied bottled gas (LPG). This created considerable social unrest of much greater magnitude that led Taguchi to develop and patent a SnO<sub>2</sub> gas sensor,<sup>59</sup> and he subsequently established the Figaro Engineering Company in 1968.<sup>60</sup>

In this current era of the Internet of Things, gas sensors can be widely used for various applications, such as industrial processes, environmental monitoring, medical diagnosis, safety, and pharmaceuticals. Resistive-based gas sensors are currently among the most widely studied gas sensors<sup>61,62</sup> and account for >20% of the gas-sensor market.<sup>63</sup> Many companies, such as Figaro, FIS, and MICS, offer this type of sensor.<sup>64</sup> Various binary, ternary,<sup>65</sup> and more complex metal oxides<sup>66</sup> have been used for the realization of resistive-based gas sensors. In general, either *n*- or *p*-type metal-oxide semiconductors can be used.<sup>67</sup> According to Kim and Lee,<sup>68</sup> SnO<sub>2</sub>, ZnO, TiO<sub>2</sub>, WO<sub>3</sub>, In<sub>2</sub>O<sub>3</sub>, and Fe<sub>2</sub>O<sub>3</sub> (with *n*-type conductivity) are the most common metal oxides used in gas sensors. This is mainly due to the high mobility of electrons in *n*-type metal oxides. The mobility of conduction electrons (*n*-type oxides) is reportedly 160, 200, and 100 cm<sup>2</sup>/(V s) for SnO<sub>2</sub>, ZnO, and In<sub>2</sub>O<sub>3</sub>, respectively.<sup>69</sup> In comparison, the mobility of the positive holes in *p*-type metal oxides is significantly lower, e.g., 0.2 cm<sup>2</sup>/(V s) for NiO.<sup>70</sup> It has been reported that the response of *p*-type metal oxides is equal

to the square root of that of n-type metal oxides with the same morphology.<sup>71</sup> This is a reason why p-type oxides are not utilized frequently as compared to n-type metal oxides. However, p-type metal oxides with good catalytic properties are used for sensing applications.<sup>72</sup> For example, p-Co<sub>3</sub>O<sub>4</sub>-decorated In<sub>2</sub>O<sub>3</sub> nanorods exhibited a good response to ethanol gas due to the high catalytic activity of p-Co<sub>3</sub>O<sub>4</sub>.<sup>73</sup> Additionally, a Cr<sub>2</sub>O<sub>3</sub>-functionalized WO<sub>3</sub> gas sensor exhibited a high response to ethanol, which was partially related to the good catalytic activation of Cr<sub>2</sub>O<sub>3</sub> to ethanol gas.

Metal-oxide gas sensors are widely employed for the detection of toxic gases and vapors for environmental control,<sup>74</sup> in the automotive industry,<sup>75</sup> in biomedical applications,<sup>76</sup> and in the food industry.<sup>77</sup> A relatively new application of gas sensors is disease diagnosis, for example, exhaled breath testing, which is a diagnostic method for the early detection of disease. This method is noninvasive, safe, and inexpensive.<sup>78</sup> Toluene, ammonia, H<sub>2</sub>S, and formaldehyde are biomarkers of lung cancer, kidney disorder, halitosis, and cardiovascular disease.<sup>79</sup> Therefore, by detecting low concentrations of these gases, the associated diseases can be diagnosed.

#### IV. OPERATION PRINCIPLE OF SEMICONDUCTOR GAS SENSORS

In a metal oxide-based sensor, i.e., a chemiresistive sensor, the change of the sensor signal is related to an ionosorption phenomenon and can be explained by a transfer of free charge carriers from the sensing layer to adsorbed surface species (or vice versa). The presence of preadsorbed species significantly affects the adsorption

process and eventually the sensing signal. Typically, a metal oxide-based sensor is operated in air, in the presence of humidity and residual gases. Under such conditions, at normal working temperatures (200–400 °C), various oxygen species (O<sub>2</sub><sup>-</sup>, O<sup>-</sup>, O<sup>2-</sup>), water, and carbon dioxide-related species are present at the surface of the metal oxide. Some species form bonds with specific surface sites (surface atoms) by exchanging electrical charge and may form dipoles, which do not affect the free charge-carrier concentration or the resistance of the sensitive layer.<sup>80</sup> Figure 1 shows a schematic of the flatband and the band-bending model of an n-type metal-oxide semiconductor gas sensor.

The modification of the overall electrical resistance of the sensitive metal-oxide layer can be caused, for example, by changes in the band bending induced by the reaction of oxygen ions with a target gas such as CO. Considering (partly) depleted layers, when the surface reactions do not affect the conduction in the entire layer (Fig. 2), the conduction process logically occurs in the bulk region, which has lower resistance relative to that the surface depleted layer. Two resistances occur in parallel: one is influenced by the surface reactions, and the other is not. Such a case can be considered a conductive layer with a reaction-dependent thickness. If a completely depleted layer exposed to reducing gases, it may be switched to the partly depleted layer due to the introduction of additional free charge carriers.<sup>81</sup>

In addition to the sensing element, the morphology of the active layer significantly affects the gas diffusion and electron transport in the layer and, therefore, directly impacts the efficiency of surface processes that determine the sensor signal. To benefit from the efficient

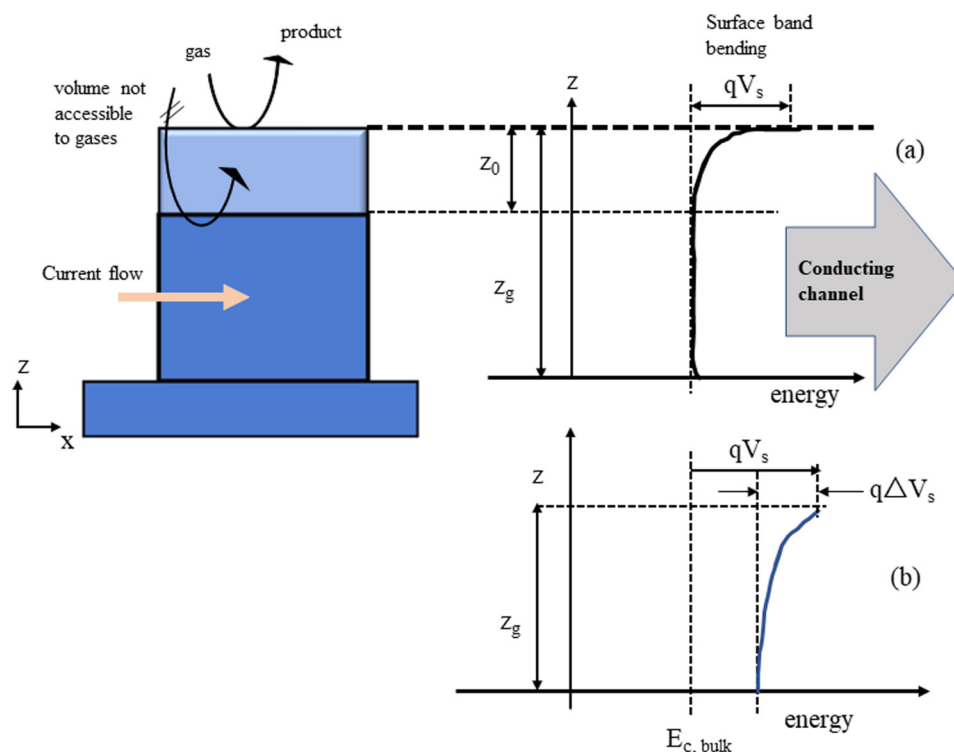


**FIG. 1.** Schematic of (a) the flatband in an n-type metal oxide and (b) a band-bending model illustrating the adsorption at the surface of the n-type metal oxide. Reproduced with permission from Barsan *et al.*, *Sens. Actuators B Chem.* **121**, 18–35 (2007). Copyright 2019 Elsevier.

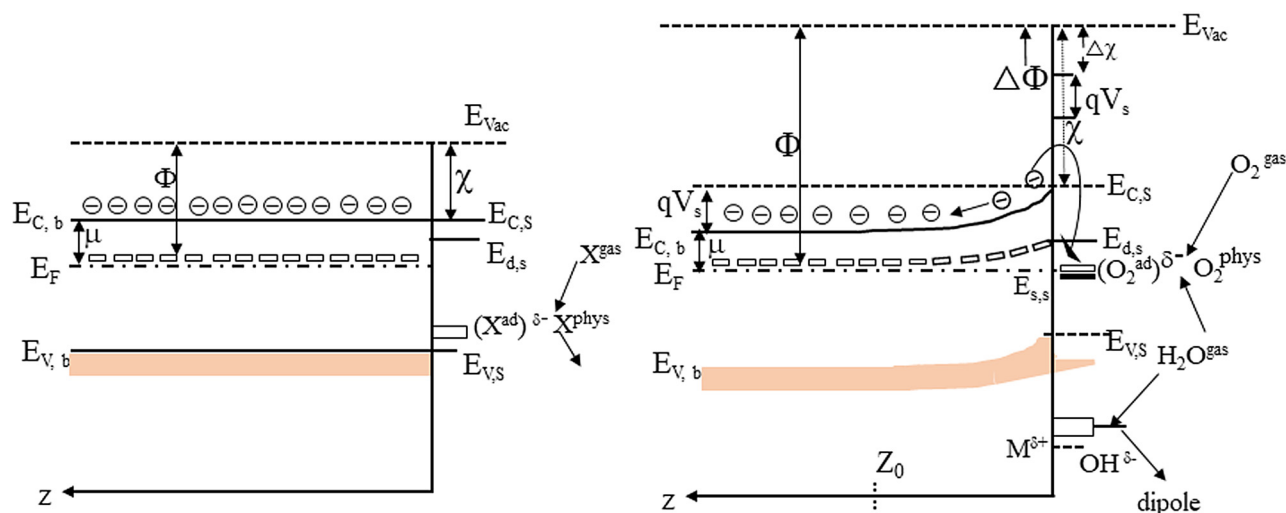


FIG. 2. Schematic of a sensing layer and energy bands, where the influence of the depleted layer on the band bending is indicated. Reproduced with permission from Barsan and Weimar, *J. Electroceram.* **7**, 143–167 (2001). Copyright 2019 Springer.

transduction of surface adsorption–desorption processes into the change of the metal-oxide conductance, the dimensions of the sensing element should be comparable to the Debye length of the material. New developments in nanotechnology allow for the easy preparation of NWs with the desired Debye length dimensions, which are attractive for gas-sensing applications.<sup>82</sup>

For n-type NWs that are widely used in sensing applications, variations of the conduction channel due to the presence of the target gas are responsible for sensing signal. Initially, in air an electron-depletion layer is formed on the outer surfaces of the NW due to the extraction of electrons by adsorbed oxygen ions. This causes the formation of a so-called conduction channel inside the core of NW. Then, depending on the interaction with either oxidizing or reducing gases, the conduction channel either contracts or expands, respectively, leading to either an increase or a decrease of NW resistance and appearance of a sensing signal.

Depending on the ratio between the characteristic transverse sizes of the nanostructures, there are two main electron-transport regimes (i) due to the presence of the adsorbed oxygen species, the number of free electrons is reduced at the oxide surface states and the electron transport is modulated by potential barriers. Thus, the gas-sensing mechanism is dependent on both the width and height of the contact potential barriers. (ii) The Fermi level is controlled by surface states under flat energy bands, and the mechanism depends mainly on the release of electrons from the surface states to the conduction band. Therefore, the influence of potential barriers, which are most significant at the contacts between agglomerates, can be neglected.<sup>83,84</sup>

## V. METAL OXIDE-BASED GAS SENSORS: DESIGN

There are many configurations available for the design of semiconductor-based gas sensors, and they can be categorized into

three major classes: (i) sintered pellet gas sensors,<sup>85</sup> (ii) thick-film gas sensors,<sup>86</sup> and (iii) thin-film gas sensor.<sup>87</sup> The use of pellet gas sensors is hindered by their limited surface area, which leads to a relatively low gas response.<sup>88</sup> Accordingly, most gas sensors are fabricated as thin or thick films, with tubular or planar configurations<sup>89</sup> (Fig. 1). Such sensors are prepared by depositing a sensitive layer on an insulating substrate. The substrate has electrodes on its surface for the readout of the sensor resistance.<sup>74,90</sup> Different techniques can be employed for the deposition of the sensing layer on the substrate, such as the sol-gel method, physical vapor deposition, chemical vapor deposition (CVD), screen printing, and spray pyrolysis.<sup>91</sup> Additionally, metallic heaters such as Pt, Pd, Ag, and Pd-Ag are often used to increase the sensor temperature to the desired value.<sup>74,90</sup> However, recently, owing to the high costs of metallic electrodes, metal-oxide electrodes, such as CuO-mixed  $\text{CaCu}_3\text{Ru}_4\text{O}_{12}$ , have been used in gas sensors.<sup>92</sup> Figure 3 shows schematics of the tubular and planar gas-sensor configurations.

Generally, alumina is used as the substrate material in gas sensors. This material has a low thermal expansion coefficient, high thermal conductivity, and high mechanical strength, along with a low price.<sup>89</sup> Additionally, flexible gas sensors have recently become popular.<sup>93,94</sup> Plastics are among the most common substrate materials, as they are flexible, lightweight, and transparent and can be mass-produced via roll-to-roll printing processes.<sup>89</sup> Furthermore, owing to the high working temperature of gas sensors, polyimide, which has a high thermal stability, has been used as a substrate material.<sup>95</sup>

## VI. CRITERIA FOR EVALUATION OF SEMICONDUCTOR GAS SENSOR

For achieving fast, reliable, and accurate detection, the basic requirements of gas-sensing materials developed for use in any



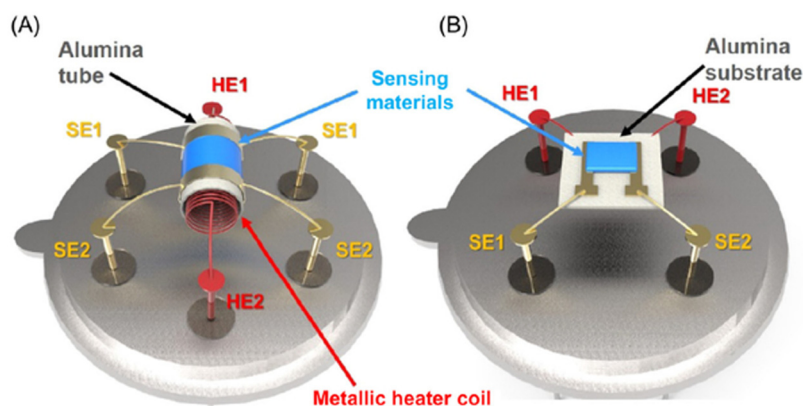


**FIG. 3.** Schematics of gas-sensor configurations: (a) tubular and (b) planar (SE and HE represent the sensor electrode and heater electrode, respectively). Reproduced with permission from Lee, *Gas Sensors Based on Conducting Metal Oxides* (2019), pp. 167–216. Copyright 2019 Elsevier.

application field are “3S” (sensitivity, selectivity, and stability). The gas-sensing performance of sensors is evaluated using a few important parameters. In this section, we define a few important sensing parameters of gas sensors.

### A. Gas response and sensitivity

The most essential parameter of a gas sensor is its response ( $R$ ) to a target gas. If a gas sensor cannot sense a target gas, it cannot be used in practice. There are different definitions of the gas response for semiconductor-based gas sensors. The response is generally defined as the ratio of the resistance variation ( $R_a/R_g$ ) or ( $R_g/R_a$ ), where  $R_a$  and  $R_g$  represent the resistances of the gas sensor in air and in the target gas atmosphere, respectively.<sup>72</sup> The former is used for n-type metal oxides in the presence of a reducing gas, such as CO or H<sub>2</sub>S, or p-type metal oxides in the presence of an oxidizing gas, such as NO<sub>2</sub>. The latter is used for n-type metal oxides in the presence of an oxidizing gas or p-type metal oxides in the presence of a reducing gas. Therefore, to calculate the response of a gas sensor, its resistance in air ( $R_a$ ) and the target gas ( $R_g$ ) should be continuously measured. This can be done using a gas-sensing measurement system, as discussed in Sec. VII. The concepts of sensitivity ( $S$ ) and response ( $R$ ) should not be confused. The sensitivity is a change in measured resistance ( $\Delta R$ ) with a change in analyte concentration ( $\Delta c$ ), i.e., the slope of a calibration graph:  $S = \Delta R/\Delta c$ . On the other hand, the response is the ratio of the sensor resistances as defined above.

### B. Response time and recovery time

In the practical application of a gas sensor, a rapid response and short recovery time are always preferred owing to the highly toxic or explosive nature of some target gases. The response time ( $R_{\text{resp}}$ ) is defined as the time required for a gas sensor to reach 90% resistance change in the presence of the target gas, and the recovery time ( $R_{\text{recv}}$ ) is defined as the time needed for the resistance of a gas sensor to return to 90% of its original baseline value after the removal of the target gas.<sup>96</sup> In some literature, 63% of the stable resistance change have also been considered the response time.<sup>97</sup> A good strategy to improve the response and recovery of gas sensors is the use of porous structures, which provide abundant channels for the diffusion of gas species.<sup>98</sup>

### C. Selectivity (cross-sensitivity)

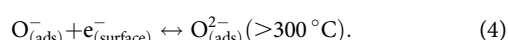
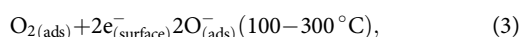
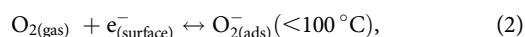
Selectivity is another critical factor for a gas sensor. It describes the ability of a sensor to differentiate a specific target gas among other interfering gases. According to Gurlo *et al.*, the selectivity ( $m_{ij}$ ) of a sensor compares the sensor signal or the sensitivity to be monitored ( $S_i/m_i$ ) to the sensor signal/sensitivity of the interfering stimulus ( $S_j/m_j$ ), which is expressed as follows:<sup>99</sup>

$$M_{ij}(c_i, c_j) = S_i/S_j \text{ and } m_{ij}(c_i, c_j) = m_i/m_j.$$

The selectivity of gas sensors should always be  $>1$ . A high selectivity corresponds to a higher response of the gas sensor to a target gas compared with the response to interfering gases.<sup>100</sup> Typically, gas sensors are sensitive to more than one gas and exhibit cross-sensitivity. Hence, obtaining a high selectivity in a gas sensor is difficult, which limits the practical applications of gas sensors.<sup>101</sup> Four common strategies for increasing the selectivity are (i) functionalization with noble-metal catalysts, (ii) tuning the sensing temperature, (iii) using heterojunctions and additives, and (iv) using filters.<sup>102</sup> In recent years, the use of metalorganic frameworks (MOFs) as membranes has attracted attention, as this new class of materials enhances the selectivity.<sup>103</sup> These materials have functional pores that can lead to the specific separation of small molecules through several types of interactions, including van der Waals interactions, metal–substrate interactions, and H bonding. Therefore, MOFs have potential for not only gas separation and storage but also gas sensing.<sup>104</sup> Because of their adjustable pore sizes, MOFs can permit the selective separation of gas molecules.<sup>104,105</sup> Therefore, the precise design of MOF coatings on the surface of sensing materials can lead to highly selective gas sensors.<sup>106</sup> For example, Weber *et al.*<sup>107,108</sup> covered ZnO NWs with a thin ZIF-8 molecular sieve membrane and reported a high selectivity to H<sub>2</sub> gas. A ZIF-8 membrane with a small pore size (3.4 Å) prevented the passage of toluene and benzene gas molecules (kinetic diameters of 5.92 and 5.27 Å, respectively), while H<sub>2</sub> molecules with a smaller kinetic diameter (2.89 Å) diffused through the ZIF-8 membrane, resulting in a high response of the gas sensor. Additionally, by using sensor arrays and multiple sensing-signal datasets, a high selectivity can be obtained.<sup>109</sup>

#### D. Sensing temperature

The operating temperature of a gas sensor determines its sensitivity. Because gas-sensing phenomena are directly related to the diffusion and reaction of target gases and are temperature-dependent, the response of gas sensing increases with the sensing temperature. Generally, the working temperature of metal-oxide gas sensors is in the range of 25–500 °C.<sup>110</sup> In this temperature range, the formation of chemisorbed oxygen ion species, such as  $O_2^-$ ,  $O^-$ , and  $O^{2-}$ , mainly depends on the variation of the temperature during gas-sensing measurements. The related equations are as follows:<sup>6</sup>



At low temperatures, the response is limited by the rates of the chemical reactions, and at high temperatures, it is limited by the diffusion rate of gas molecules. At intermediate temperatures, the rates of adsorption and desorption become equal, yielding the highest response. Each gas sensor has an optimal sensing temperature, which depends on the target gas, chemical composition, and morphology.<sup>111</sup> From an energy viewpoint, lower sensing temperatures are favorable because they require lower power consumption and allow the application of the gas sensor in remote areas. However, for some applications, e.g., ammonia production, which generally occurs above 450 °C, high-temperature gas sensors are required.<sup>112</sup>

#### E. Limit of detection (LOD)

The detection limit can be defined as the lowest concentration of gas that can be detected at a certain temperature. The limit of detection can be expressed as follows:<sup>99</sup>

$$\text{LOD} = C_{\min} = f^{-1}(R_{\min}), \quad R_{\min} = R_0 + 3\sigma_0, \quad (5)$$

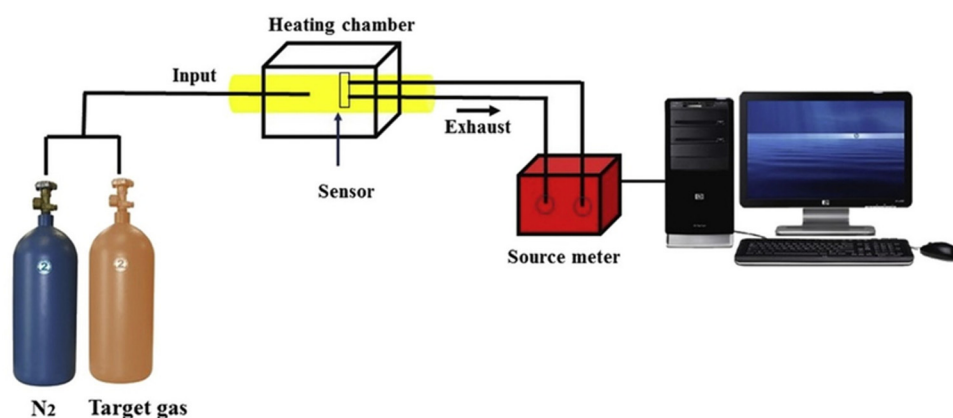


**FIG. 4.** Schematic of a dynamic gas-sensing system. Reproduced with permission from Bonyani *et al.*, *Thin Solid Films* **636**, 257–266 (2017). Copyright 2019 Elsevier.

where  $f^{-1}(R)$  is the inverse of the calibration function  $f(C)$  and  $C_{\min}$  represents the minimum detectable gas concentration. The minimum sensor response ( $R_{\min}$ ) is typically chosen as three times the standard deviation of the  $\sigma_0$  response, which is considered the noise of the measurement. In other words, the LOD can be simply calculated as “ $3 \times \text{noise}_{\text{rms}}/\text{slope}$ ,” where  $\text{noise}_{\text{rms}}$  represents the standard deviation of the sensor signal, and the slope is the first derivative of the response vs the gas concentration.<sup>113,114</sup> For further details regarding the typical measurement used to characterize the gas-sensor performance, the reader is referred to a previous work.<sup>99</sup>

#### VII. MEASUREMENT SYSTEMS

There are two main types of systems for gas-sensing measurement: dynamic and static. Regardless of the type of measurement system, the device requires gas valves and gas-flow controllers for the injection of the target gas into the gas chamber, which is equipped with a gas inlet and outlet. The sensing temperature should be controllable, and a gas chamber with a limited volume to avoid long response times is typically preferred. Finally, the measurement system should be connected to a computer to continuously register the resistance of the sensor in different atmospheres.<sup>18</sup>

In a dynamic system (Fig. 4), predetermined gas concentrations with constant flow rates flow to the gas chamber through tubes, and the flow is regulated by mass flow controllers.<sup>115</sup> The sensors inside the gas chamber are connected to a measurement unit to record the resistance variation continuously. During gas-sensing tests, the resistances of the sensor in air and in the presence of different concentrations of the target gas at different temperatures are recorded.

In a static gas-sensing measurement system (Fig. 5), the sensor is placed in a gas chamber with an adjustable temperature and humidity.<sup>116</sup> During the gas-sensing test, a predetermined amount of the target gas is injected into the test chamber through the gas inlet by a gas-injection unit. When the sensor resistance becomes stable, the gas chamber is opened for the sensors to recover in air. This procedure is repeated for different gas concentrations and at different temperatures, and a curve indicating the variation of the sensor resistance vs time in different atmospheres is obtained.

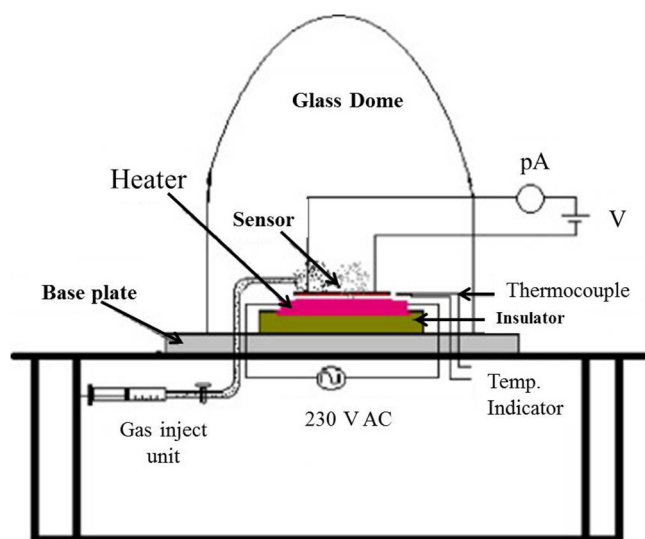


**FIG. 5.** Schematic of a static gas-sensing system. Reproduced with permission from Patil *et al.*, *Sens. Actuators B Chem.* **126**, 368–374 (2007). Copyright 2019 Elsevier.

### VIII. NW-BASED GAS SENSORS: GENERAL OVERVIEW

A decrease in the sensor size results in lower power consumption (due to a small thermal mass), easier mass production, faster heating, and easier integration with small chips.<sup>89</sup> Nanoscale materials not only exhibit the aforementioned advantages but also have a large effective area, which enhances the gas-adsorption phenomena. When the size reaches  $\lambda_D$  (Debye length), the surface energy significantly increases, and agglomeration easily occurs, reducing the surface area.<sup>72</sup> One effective approach for overcoming the agglomeration is to engineer the surface at the nanoscale to increase the surface area of the gas sensor.<sup>117</sup> Various nanostructures, such as NWs,<sup>118,119</sup> nanofibers,<sup>120,121</sup> nanorods,<sup>122,123</sup> nanotubes,<sup>124,125</sup> hierarchical structures,<sup>126,127</sup> hollow structures,<sup>128–130</sup> nanobelts,<sup>131,132</sup> mesoporous structures,<sup>133,134</sup> and core-shell (C-S) structures,<sup>135,136</sup> have been investigated for gas-sensing devices.

By definition, nanostructures with cross section sizes between 2 and 200 nm and microscale lengths are NWs.<sup>137</sup> Using metal-oxide NWs for the realization of gas sensors has advantages, such as a very high surface-to-volume ratio, small dimensions, high stability, high crystallinity, facile preparation methods, minimal power consumption, and ease of functionalization with catalysts for sensing studies.<sup>69,138,139</sup> Accordingly, NW gas sensors have been used for not only the realization of gas sensors<sup>140,141</sup> but also the fabrication of various biosensors.<sup>142</sup> In Sec. IX, we discuss the synthesis of NWs and their performance as gas sensors.

### IX. SYNTHESIS OF METAL-OXIDE NWS

In general, the successful growth of NWs needs two dimensions to be restricted to the nanometer scale, while the third one should be extended to macroscopic dimensions.<sup>143</sup> The most

common method for synthesizing metal-oxide NWs with a random alignment is the bottom-up approach, which can be classified into solution-phase growth and vapor-phase (solid-state) growth techniques. These include solution-based techniques or template growth and synthesis via vapor-phase transport or CVD. The advantages of these methods include the high purity and small diameters of the synthesized materials, low-cost synthesis, and the ease of doping and homojunction or heterojunction formation.<sup>138</sup> The main disadvantage of solution-based growth is the agglomeration of the NWs. The most common method for the synthesis of NWs is vapor-liquid-solid (VLS) growth, which is briefly explained as follows.

#### A. VLS growth

Bottom-up VLS growth was introduced by Wagner and Ellis at Bell Laboratories to describe the growth of Si whiskers in the presence of a liquid Au droplet.<sup>136,144</sup> Compared with other growth techniques, the VLS method is simple and inexpensive and can produce NWs with a high aspect ratio.<sup>145</sup> Generally, a metallic catalyst is used for VLS growth. The catalyst acts as a reservoir for atomic species and induces the crystallization of the NWs.<sup>146</sup> Generally, at a fixed temperature, the length of the NWs depends on the growth time, and the NW diameter is determined by the size of the metal catalyst droplets. If the catalyst droplet size has a narrow distribution, NWs with a uniform diameter can be obtained.

During a typical VLS growth technique, metal catalysts are first melted into liquid alloy droplets. The liquid surface should have a large accommodation coefficient to be considered a preferred site for the absorption of vapor species of the NW materials. Being supersaturated with the gas-phase reactants of the NW materials, NW growth occurs via precipitation at the solid-liquid interface. Then, when the alloy droplets become supersaturated, the source metal precipitates, and metal oxides are grown under the  $O_2$  flow. As-synthesized metal oxides are grown along a particular orientation, leading to the formation of 1D NWs.<sup>147</sup> A good catalyst should form a liquid alloy with the NW material; and in the ideal situation, it should be able to form an eutectic alloy. The growth temperature should be higher than the eutectic point but lower than the melting point of the NW material. Both physical methods (including thermal evaporation, laser ablation, and arc discharge) and chemical methods can be used to generate the vapor species required during the NW growth.<sup>147</sup>

For the growth of  $TeO_2$  NWs, the Au-catalyzed VLS growth technique was employed, as shown in Fig. 6. Au nanoparticles (NPs) were deposited on a substrate on which  $TeO_2$  NWs were grown. With the increasing amount of Te vapor condensation and dissolution, Te and Au formed a liquid. With the decrease in the temperature and in the presence of  $O_2$ , the  $TeO_2$  crystals nucleated, and further condensation/dissolution of Te vapor increased the amount of  $TeO_2$  crystal precipitation from the alloy. The incoming Te species diffused and condensed at the existing solid/liquid interface. Consequently, no new solid/liquid interface was formed, and the interface was pushed to form  $TeO_2$  NWs. After cooling, the alloy droplets solidified on the  $TeO_2$  NW tips.<sup>148,149</sup> The reverse variation of the VLS technique is the solid-liquid-vapor (SLV)



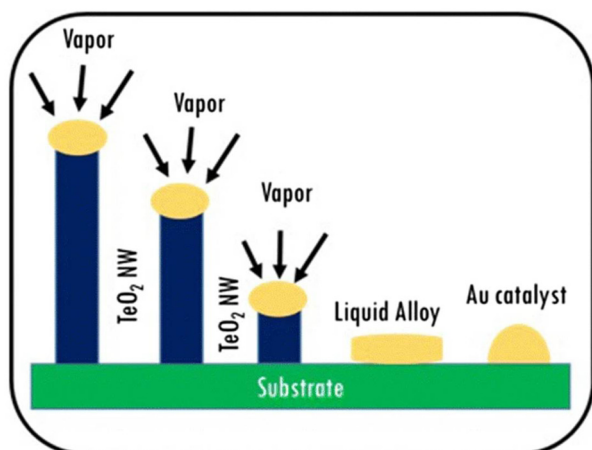


FIG. 6. Schematic of the VLS growth mechanism for TeO<sub>2</sub> NWs. Reproduced with permission from Kim *et al.*, *Met. Mater. Int.* **25**, 805–813 (2018). Copyright 2019 Springer.

growth method, in which etching is used to form “negative NWs,” which are hollow in nature, in a single crystal.<sup>150</sup>

## B. Synthesis of branched NWs

Branched NWs, which are also called nanoforests or nanotrees, have a three-dimensional (3D) morphology with numerous homojunctions or heterojunctions and direct electron-transport pathways. Compared with NPs and 1D NWs, 3D branched NWs are superior with regard to the structural hierarchy and surface area,<sup>151</sup> making them suitable for gas sensing and even for the detection of gases at sub-parts per million levels.<sup>152</sup> Additionally, branched NWs offer increased conduction paths and enhanced conduction between the NW branches and backbones.<sup>153</sup> Many methods can be used for the synthesis of branched NWs. The typical methods include sequential VLS solution growth on primary NWs, self-catalytic growth, and screw-dislocation in combination with VLS.<sup>154</sup> The most common method is VLS, which consists of three steps: VLS growth of the primary NWs, deposition of the metal catalyst onto the as-grown NWs, and second VLS growth of the branched NWs. The density of the NW branches is directly related to the amount of the catalyst particles deposited on the primary NWs, and the length of the branches depends on the growth time.<sup>151</sup> Therefore, via VLS growth, branched NWs with the desired features and high crystal quality can be synthesized. However, the synthesis temperature for VLS and most vapor-phase growth methods is high, and some of them require expensive facilities.<sup>151</sup>

## C. Synthesis of C-S NWs

C-S NWs are a subcategory of composite materials and contain an NW core coated with a shell of a different material. Therefore, C-S NWs are synthesized through the coating of an original core with a shell of another material. The properties of C-S

NWs can differ from those of the core and shell materials.<sup>155</sup> The ideal synthesis method should be not only compatible with the procedure for fabricating the gas sensor but also able to easily deposit the shell with high crystallinity and controlled thickness onto the core material. Additionally, it should have minimal detrimental effects on the gas-sensing performance of C-S NWs and be cost-effective, clean, and safe.<sup>155</sup>

Compared with top-down methods, bottom-up methods for the synthesis of C-S NWs can yield significantly finer structures and minimize the energy loss.<sup>156</sup> Among the various techniques that can be employed for the deposition of a shell material on primary core NWs, such as CVD and laser-induced assembly, the most precise and reliable method is atomic layer deposition (ALD), which allows excellent control over the shell thickness.<sup>157</sup> ALD is a vapor-phase technology based on the sequential use of self-limiting chemical reactions. This technique can produce inorganic nanomaterials such as oxides,<sup>158</sup> nitrides,<sup>159,160</sup> and metals,<sup>161</sup> with a subnanometer level of thickness control.<sup>162,163</sup> The main benefits of ALD are the excellent control of the thickness, the excellent uniformity, and the conformality over the substrate surface, which makes this technique advantageous for the coating of 1D materials such as NWs.<sup>164–167</sup> The shell layers produced by ALD are extremely smooth, continuous, pinhole-free, and conformal to the original core, because the reactions are self-limiting and saturated.<sup>163</sup> Figure 7 shows schematics of different techniques for the growth of NWs.

## X. SINGLE-NW GAS SENSORS

Even though the development of single NW-based gas sensors is challenging, there are many reports on the sensing properties of these sensors.<sup>167–169</sup> The sensing properties of single NWs are affected by the NW diameter, the NW synthesis procedure, and the reactions that occur on the NW surfaces.<sup>170</sup> Realization of single-NW gas sensors has significant fabrication issues, e.g., the formation of electrical contacts. Electron-beam lithography can be used to define the electrical contacts for a single-NW gas sensor. However, a simpler method is synthesis, sonification, and dispersal of the NW on another substrate equipped with electrodes. Because of the complex fabrication processes, the commercialization of single-NW gas sensors is very difficult.<sup>171</sup>

Tonezzer and Hieu<sup>170</sup> prepared monocrystalline SnO<sub>2</sub> NWs via CVD. They were subsequently dispersed onto a substrate, and by applying electrical contacts, single-NW gas sensors with different diameters were fabricated for NO<sub>2</sub>-sensing studies (Fig. 8).

Figure 9(a) shows the response of single-NW gas sensors at the optimal temperature (200 °C). A smaller NW diameter yielded a higher response of the gas sensor. The response to NO<sub>2</sub> gas has the following relationship with the diameter ( $R$ ) of the NW and the depth of the depleted zone ( $L_D$ ):<sup>170</sup>

$$\text{Response} = \text{Constant} \times \left( \frac{R}{R - L_D} \right)^2. \quad (6)$$

As shown in Fig. 9(b), a smaller NW diameter yielded a higher response of the gas sensor to NO<sub>2</sub>. Because  $L_D$  was constant for all the NW gas sensors, the reduction of the NW diameter

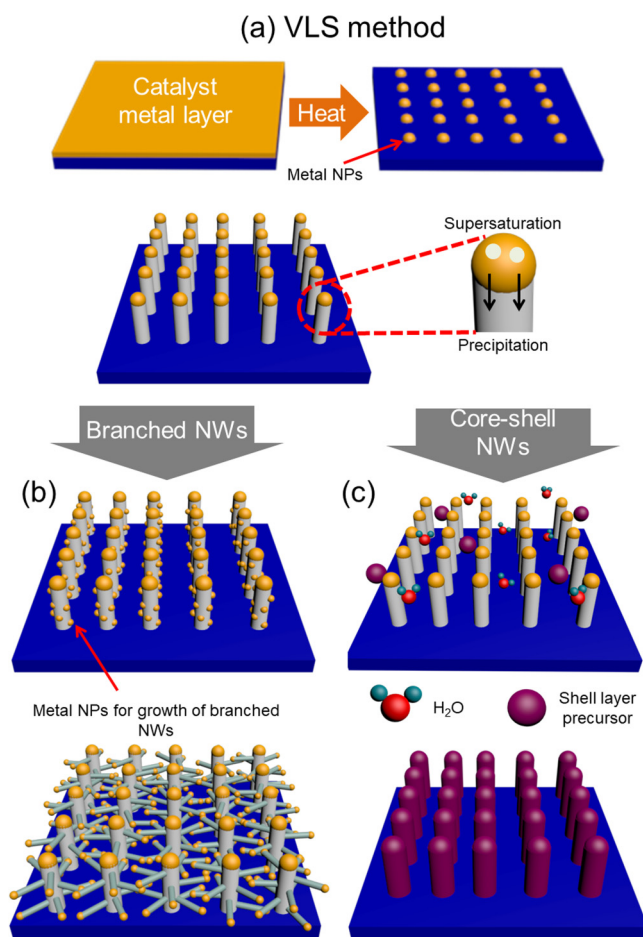


**FIG. 7.** Schematics of different techniques for the growth of NWs: (a) VLS method; (b) branched-NW growth; and (c) C-S NW growth.

resulted in a higher gas response because of the higher ratio of the cross sections of the conducting NW. Additionally, because the gas sensors had different charge-carrier densities, they exhibited different LODs, as shown in the inset of Fig. 9(a).

The foregoing results were confirmed by Lupan *et al.*<sup>172</sup> The responses of single ZnO NW (100 and 200 nm in diameter) gas sensors were directly related to the diameter of the NW, and the highest gas response was observed for a sensor with an NW diameter of 100 nm. In a gas sensor with a smaller NW diameter, the diameter and Debye length were comparable, resulting in significant resistance modulation and a higher response.<sup>172</sup> In another study, the responses of single SnO<sub>2</sub> NW gas sensors with different diameters (20–140 nm) were proportional to the inverse of the diameter; the smallest NW diameter yielded the highest gas response.<sup>173</sup>

In general, single-NW gas sensors have inferior sensing properties to multiple- and networked-NW gas sensors. This is likely because of the large number of homojunctions in

networked and multiple NWs, which act as powerful sources of resistance modulation. In this regard, Zhang *et al.*<sup>174</sup> synthesized a single In<sub>2</sub>O<sub>3</sub> NW gas sensor via a laser-ablation method. The sensor exhibited a response to parts per billion-level NO<sub>2</sub> concentrations at ~25 °C. However, the response of a multiple-NW gas sensor was not only higher but also more reliable. Furthermore, the fabrication procedure for the multiple-NW gas sensor was simpler.<sup>174</sup> The addition of noble metals at the surfaces of single-NW gas sensors has been examined. Single ZnO NWs, which were partially coated with Pt clusters, exhibited good sensitivity and selectivity to H<sub>2</sub> gas at room temperature—far better than the sensitivity and selectivity of an uncoated sensor.<sup>173</sup> Additionally, the power consumption of the single-NW gas sensor was significantly lower than that of multiple ZnO NWs.<sup>175</sup>

## XI. BRANCHED-NW GAS SENSOR

A high-performance NO<sub>2</sub> gas sensor based on Bi<sub>2</sub>O<sub>3</sub> branched SnO<sub>2</sub> NWs was reported by Bang *et al.*<sup>176</sup> The SnO<sub>2</sub> NWs and Bi<sub>2</sub>O<sub>3</sub> branches were simultaneously produced via the VLS method. The sensor exhibited a high response of 56.92 to 2-ppm NO<sub>2</sub> gas. The high sensing performance of the branched-NW sensor was related to the large surface area of the sensor resulting from the Bi<sub>2</sub>O<sub>3</sub> branching and the formation of Bi<sub>2</sub>O<sub>3</sub>–Bi<sub>2</sub>O<sub>3</sub> and SnO<sub>2</sub>–SnO<sub>2</sub> homojunctions and Bi<sub>2</sub>O<sub>3</sub>–SnO<sub>2</sub> heterojunctions.

CuO-functionalized SnO<sub>2</sub> branched NWs were realized via a single process by using Cu as a catalyst for the growth of SnO<sub>2</sub> branches and the source of CuO NWs. Using this method, Kim *et al.*<sup>177</sup> fabricated NWs CuO-functionalized SnO<sub>2</sub> branched NWs. After annealing at 700 °C, CuO was located at the tips of the SnO<sub>2</sub> branches. When the gas sensor was exposed to H<sub>2</sub>S, a high response was observed, which was mainly related to the conversion of semiconductive CuO into metallic CuS, which induced significant resistance modulation. However, because the CuO-induced depletion region covered a considerable volume of the SnO<sub>2</sub> branches, there were no electrons available for incoming NO<sub>2</sub> gas molecules, resulting in a low response to NO<sub>2</sub> gas.<sup>177</sup>

Kim *et al.*<sup>178</sup> prepared ZnO branched SnO<sub>2</sub> NWs via a VLS growth method and then sputtered NWs with a Co shell, followed by annealing treatment to convert the Co layer into Co NPs at the surfaces of the ZnO branches [Figs. 10(a) and 10(b)]. Figures 10(c) and 10(d) show schematics of the sensing mechanism in branched-NW gas sensors with and without Co functionalization, respectively. The NO<sub>2</sub> gas molecules with a highly oxidizing nature captured electrons from ZnO branches, increasing the resistance of the gas sensors. However, for the Co-functionalized sensors, owing to the spillover effect of Co, NO<sub>2</sub> gas species were first absorbed on the active sites of Co NPs and then migrated to the ZnO surfaces, increasing the resistivity. Furthermore, because of the difference between the work functions of n-ZnO and metallic Co, a Schottky potential barrier formed at the interfaces between ZnO and Co. In the NO<sub>2</sub> atmosphere, the gas molecules captured electrons from Co, leading to the enlargement of the electron-depletion layer in ZnO and contributing to the sensor signal.

Woo *et al.*<sup>179</sup> prepared highly porous ZnO NWs via Au-assisted VLS growth. Through the cation-exchange reaction due to the thermal evaporation of CoCl<sub>2</sub> powder, as-grown ZnO NWs

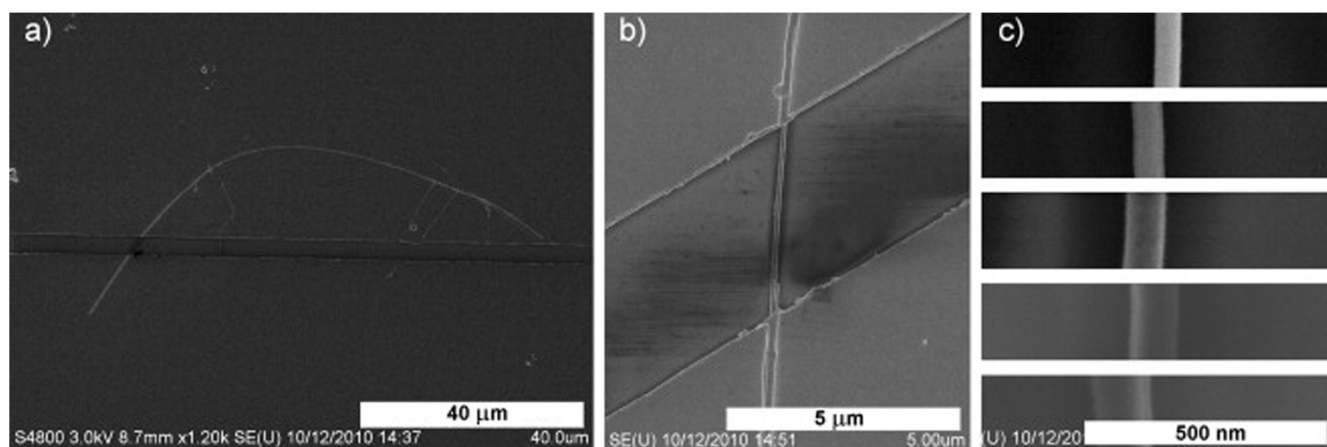


**FIG. 8.** (a) and (b) Scanning electron microscopy images of a single NW (c) and of NWs with different diameters (from the bottom to the top: 117, 103, 78, 62, and 41 nm). Reproduced with permission from *Sens. Actuators B Chem.* **163**, 146–152 (2012). Copyright 2019 Elsevier.

were transformed into CoO NWs. The corresponding reaction resulted in the growth of codeposited ZnO branches (Fig. 11). The presence of numerous homojunctions in the ZnO NW branches resulted in a higher initial resistance compared with the pristine ZnO NWs. Therefore, in a p-xylene atmosphere, a large modulation of the resistance due to the release of electrons led to a high response of the gas sensor. Additionally, the high response to

p-xylene was related to the catalytic activity of Co, which facilitated the dissociation of the less reactive p-xylene into reactive smaller gases. In a similar study, Ni-doped branched ZnO NWs were grown via a similar procedure. They exhibited a high gas response to 5-ppm p-xylene ( $R_a/R_g = 42.44$ ) at 400 °C, which was significantly higher than the response to other gases. The high selectivity of the gas sensor was related to the catalytic activity of Ni.<sup>180</sup> An

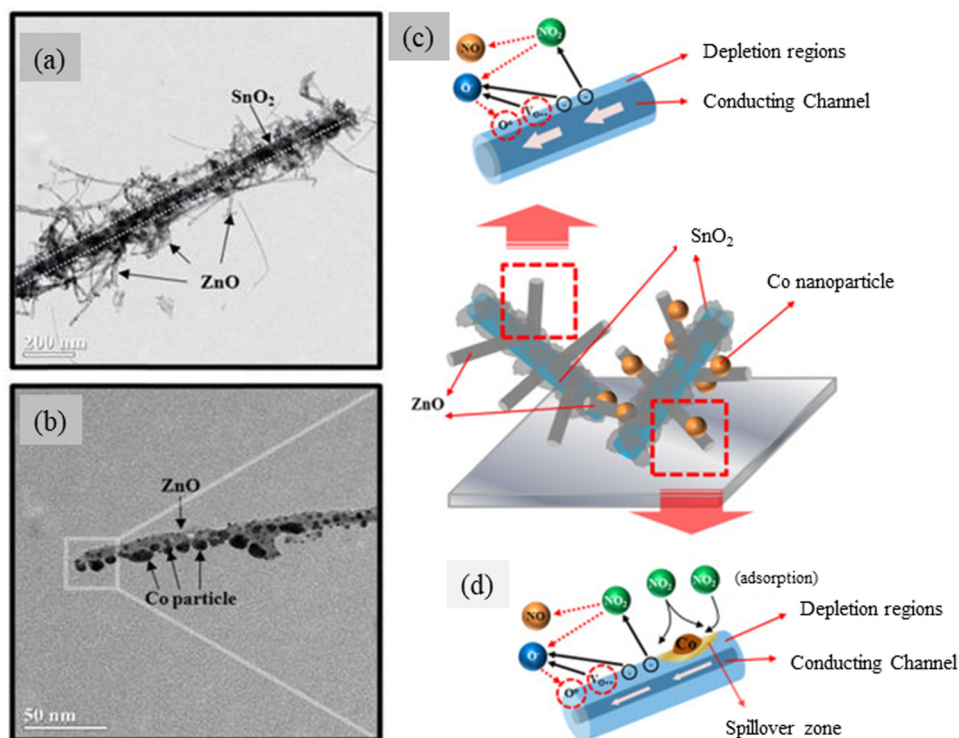


**FIG. 9.** (a) Gas responses of the five single-NW sensors to various concentrations of NO<sub>2</sub> gas. The inset shows the LOD for different single-NW gas sensors. (b) Gas response vs NW diameter. Reproduced with permission from Tonezzer and Hieu, *Sens. Actuators B Chem.* **163**, 146–152 (2012). Copyright 2019 Elsevier.



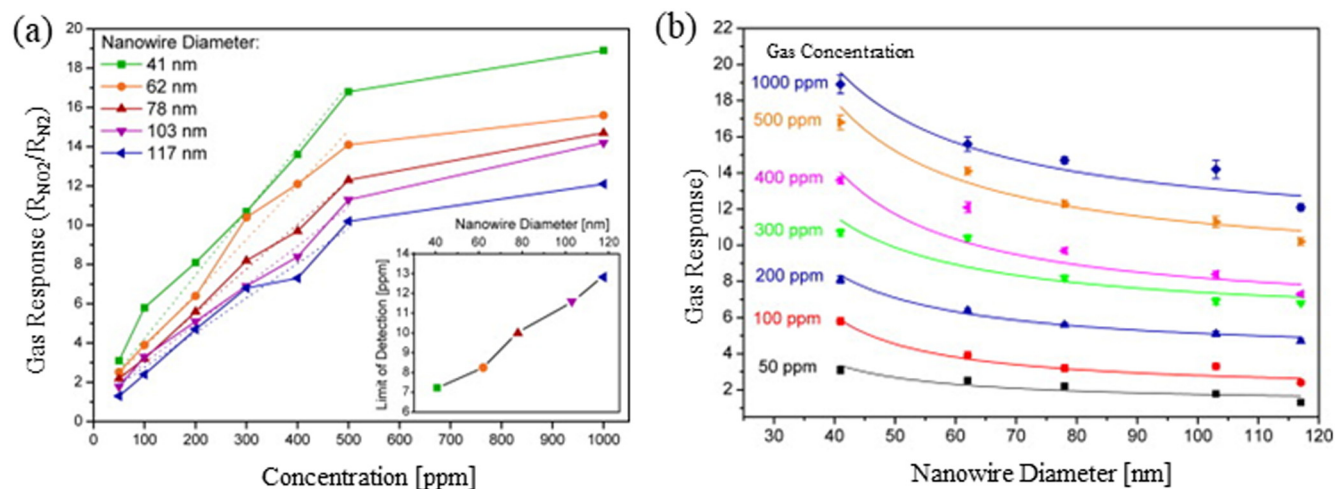


**FIG. 10.** Transmission electron microscopy images showing (a) ZnO branches and (b) Co particles. Schematic of the sensing mechanisms (c) without and (d) with Co functionalization. Reproduced with permission from Kim *et al.*, *Sens. Actuators B Chem.* **219**, 22–29 (2015). Copyright 2019 Elsevier.

*et al.*<sup>153</sup> synthesized branched ZnO NWs using Au-assisted VLS growth. An enhanced response to NO<sub>2</sub> gas compared with an unbranched sensor was achieved due to the 3D porous structure and the large surface area resulting from the formation of branches, along with the presence of abundant ZnO–ZnO homojunctions in the branched morphology.

#### A. Potential of NWs for next-generation sensing

The selection of an optimal active sensing material is challenging. In recent years, advancements in nanotechnology have allowed for the synthesis of a large variety of new materials with tunable properties, which can be employed for numerous applications,

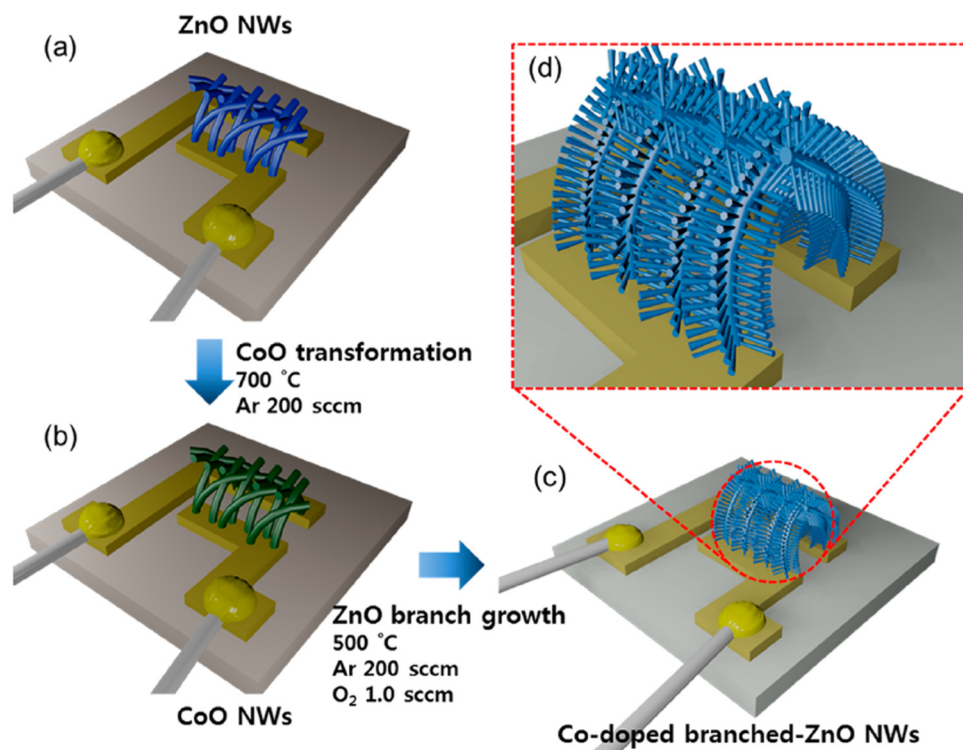


**FIG. 11.** (a) ZnO NWs; (b) transformation of ZnO NWs into CoO NWs; (c) and (d) Co-doped ZnO NW branches. Reproduced with permission from Woo *et al.*, *ACS Appl. Mater. Interfaces* **6**, 22553–22560 (2014). Copyright 2019 American Chemical Society.

including sensing.<sup>181–183</sup> Lately, nanostructures have attracted considerable attention, particularly NWs. Low-dimensional systems, along with functional nanostructured arrays, can play a key role in many devices.<sup>184–186</sup> Such nanostructures can allow both efficient transport of electrons and optical excitation, which can be useful for next-generation sensing devices. Because of their tunable electron-transport properties and their very high surface-to-volume ratio, their electrical properties are significantly influenced by minor perturbations.<sup>184</sup> Among the various nanostructures, NWs exhibit unique properties, such as mechanical stability, lightness, enhancement of the electrical current, and potential reduction, which are very useful for the development of efficient sensors. The value of sensors is based on their selectivity and sensitivity, which can be strongly enhanced by NW-modified electrodes in the sensor devices. Therefore, NW arrays are among the most fascinating and promising materials in the field of nanosensing.<sup>183,184</sup> Their properties can be precisely controlled by manipulating the synthesis conditions and using well-developed techniques, and the native oxide layer naturally present on the outside of the NWs allows the use of many well-developed functionalization methods and chemistries.<sup>187–189</sup> Consequently, NWs are excellent candidates for next-generation sensing materials, as long as the sensing platforms are optimally designed.

## XII. C-S NW GAS SENSORS

C-S composites have attracted special attention in many areas, including catalysis and electrocatalysis,<sup>173</sup> as well as different types of sensors.<sup>190,191</sup> Karnati *et al.* comprehensively discussed the different aspects of the sensing mechanism of C-S NW gas sensors.<sup>155</sup> For gas-sensing applications, an optimal shell thickness is generally needed to achieve the highest gas response in C-S NWs. This was confirmed by Kim *et al.*,<sup>192</sup> who reported the sensing performance of p-n CuO-ZnO C-S NWs with shell thicknesses of 5–110 nm. The gas-sensing results indicated an enhanced response to both C<sub>6</sub>H<sub>6</sub> and CO gases at a shell thickness of 35 nm, which was comparable to the Debye length ( $\lambda_D$ ) of ZnO. For ZnO shells thinner than  $\lambda_D$  of ZnO, all electrons were completely depleted [Fig. 12(a)], and in the presence of CO and C<sub>6</sub>H<sub>6</sub> gases, the released electrons significantly modulated the sensor resistance. For shells thinner than  $\lambda_D$ , because the shell volume was significantly smaller than the total volume of the C-S NWs, the negligible resistance modulations did not significantly affect the sensing response. Additionally, for thick shells, only a portion of the shell experienced the resistance variations in air and target gas atmospheres, resulting in a low response of the gas sensor [Fig. 12(b)].

In a similar study, the effect of shell-thickness optimization on the performance of SnO<sub>2</sub>-Cu<sub>2</sub>O C-S NWs with various shell thicknesses (5–80 nm) was investigated.<sup>193</sup> A gas sensor with a shell thickness of 30 nm revealed an enhanced gas response to reducing gases, whereas a pristine gas sensor exhibited a better response to NO<sub>2</sub> gas. The degree of resistance modulation of the outer layer of Cu<sub>2</sub>O, which was directly exposed to air, varied inversely with respect to the shell thickness. Therefore, a thicker shell was only partially modulated. In contrast, even though very thin shells completely experienced the resistance modulation, the fraction of

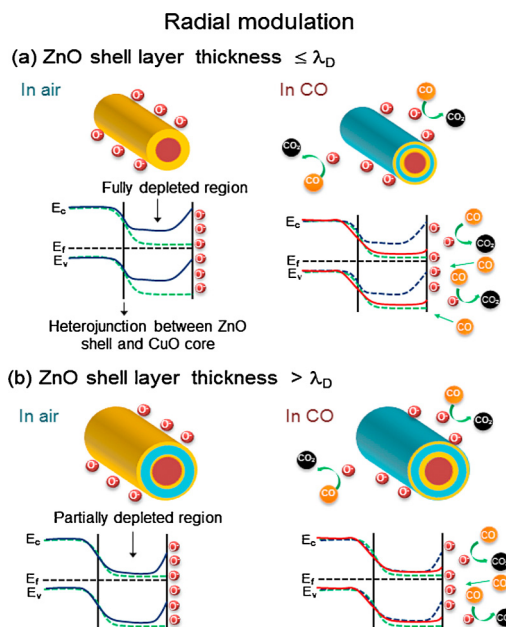


**FIG. 12.** Sensing mechanism of CuO-ZnO C-S NWs: (a) ZnO thickness smaller than the Debye length; (b) ZnO thickness larger than the Debye length. Reproduced with permission from Kim *et al.*, *Sens. Actuators B Chem.* **222**, 249–256 (2016). Copyright 2019 Elsevier.

the shell relative to the total volume of C-S NWs was negligible, resulting in a low response. Regarding the fraction of shell layers in the total volume of the n-p C-S NWs (which was proportional to the shell thickness), the response exhibited a bell-shaped curve with respect to the shell thickness (Fig. 13). A 30-nm-thick shell exhibited a high gas response. Additionally, for C-S NWs, the presence of the p-n interface, which acted as a blocking layer, limited the expansion of the Cu<sub>2</sub>O layer. Accordingly, less resistance modulation for NO<sub>2</sub>, which is an oxidizing gas, occurred, resulting in a low response to NO<sub>2</sub>.

In another study, the optimal shell thickness was verified for SnO<sub>2</sub>-ZnO C-S NWs (shell thicknesses of 3.5–95 nm), which were fabricated via VLS and ALD.<sup>194</sup> The sensor with a shell thickness of 40 nm exhibited the highest response to the reducing gases. As shown in Fig. 14(a), the resistance due to the radial modulation of the electron-depleted shell varied according to the shell thickness. Figure 14(b) shows the electric-field smearing effect. For shell layers thinner than  $\lambda_D$ , electron pathways were present in both the shell and core materials. This increased the resistance modulation in the C-S NWs. Even though a fully electron-depleted shell experienced a large resistance change, a noticeable portion of the electron pathways passed through the inner core, resulting in a negligible resistance change for the C-S NWs. Additionally, for thick shells, the resistance change in the C-S NWs upon exposure to reducing gases was determined only by the partial radial modulation of the electron-depleted shell, resulting in a low response. As shown in Fig. 14(c), the optimal shell thickness resulted in the best sensing response.



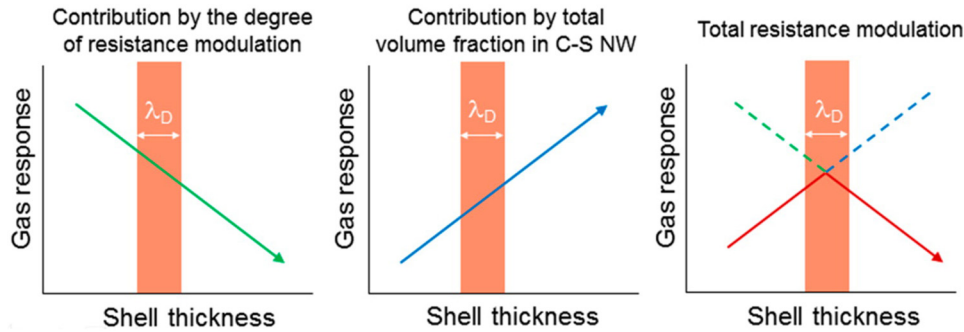


**FIG. 13.** Total resistance modulation of the C-S NWs in the presence of reducing gases. Reproduced with permission from Kim *et al.*, ACS Appl. Mater. Interfaces 7, 15351–15358 (2015). Copyright 2019 American Chemical Society.

The Debye length indicates the penetration depth of charge-carrier redistribution.<sup>195</sup> It can be calculated as follows:<sup>196</sup>

$$\lambda_D = \sqrt{\frac{\epsilon k_B T}{q^2 n_0}}, \quad (7)$$

where  $\lambda_D$  represents the Debye length,  $\epsilon$  is the static dielectric constant,  $k_B$  is the Boltzmann constant,  $T$  represents the absolute temperature,  $q$  represents the electrical charge of the carrier, and  $n_0$  represents the carrier concentration.

With regard to gas sensing, the Debye length is used to describe the charge-carrier transfer between base materials and heterostructure materials or adsorbed gas species. Depletion-layer formation is one of the most useful phenomena related to gas sensing. In C-S structures, the control depletion-layer formation can be done by adjusting the radius of the core to be approximately equal to the Debye length. One strategy for increasing the sensing performance of a C-S structure to reducing gases is the selection of n-type materials to induce charge-carrier transfer from the shell layer to the core layer. This allows adsorbed oxygen to completely deplete the remaining carriers in the shell layer, causing a large change in the sensor resistance upon exposure to reducing gases. However, it should be noted that the optimal thickness for these C-S-type sensors must be determined according to the Debye lengths of the two materials.<sup>195</sup> In the literature, the Debye lengths of different materials have been reported. Table I presents the Debye lengths of commonly used sensing materials.

### XIII. NOBLE METAL-FUNCTIONALIZED AND HETEROJUNCTION NW GAS SENSORS

A very promising approach to enhance the overall performance of gas sensors is functionalization or decoration with different noble metals. In general, noble metals such as Pt,<sup>210</sup> Pd,<sup>211</sup> Au,<sup>212</sup> Rh,<sup>213</sup> and Ag<sup>214</sup> dispersed on the surface of the sensing layer can enhance the adsorption of target gases and their subsequent interaction with adsorbed oxygen species. Therefore, functionalized metal-oxide NWs have attracted considerable attention.<sup>215</sup> Different methods, including gamma-ray irradiation,<sup>216</sup> ultraviolet (UV) irradiation,<sup>211</sup> sputtering,<sup>217</sup> and thermal evaporation,<sup>218</sup> can be used for introducing noble metals into oxide semiconductors.

When a noble metal is functionalized on the surface of metal oxides, owing to the different work functions, charge transfer

occurs until the Fermi levels are equalized. Assuming that electrons migrate from the metal oxides to the noble metals, which is often observed in noble metal oxide-functionalized gas sensors, electrons accumulate in the noble metal, increasing the width of the electron-depletion layer in the metal oxide. Schottky potential

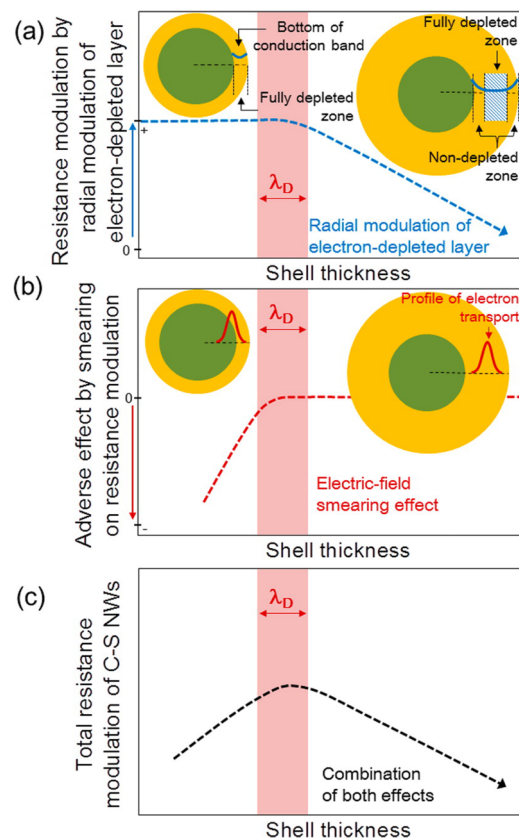


**FIG. 14.** (a) Resistance modulation by radial modulation of the electron-depleted shell; (b) adverse effect of smearing on the resistance modulation; (c) total resistance modulation. Reproduced with permission from Choi *et al.*, ACS Appl. Mater. Interfaces 6, 8281–8287 (2014). Copyright 2019 American Chemical Society.

TABLE I. Debye length of commonly used sensing materials.

Material	Debye length (nm) at T (°C, unless otherwise specified)	Reference
SnO <sub>2</sub>	3.2 at 300	196
Co <sub>3</sub> O <sub>4</sub>	3.8 at 300	196
Undoped SnO <sub>2</sub> (obtained by wet chemistry)	3.6 at 300	197
Undoped SnO <sub>2</sub> (flame spray pyrolysis)	>91 nm at 300	197
Sb doped SnO <sub>2</sub> (flame spray pyrolysis)	1 at 300	197
ZnO	5 at 300	198
ZnO	27 at 1000 K	199
SnO <sub>2</sub>	~2 nm to ~200 nm at 300 °C	200
ZnO	30 at T not mentioned	201
ZnO	21.7 at 300	202
Nb <sub>2</sub> O <sub>5</sub>	28 at T not mentioned	202
In <sub>2</sub> O <sub>3</sub>	1 at T not mentioned	203
Fe <sub>2</sub> O <sub>3</sub>	12.3 at 313 K	204
NiO	1 at T not mentioned	205
NiO	30 at 300	206
TiO <sub>2</sub>	11 at 250	207
CuO	12.7 at T not mentioned	208
WO <sub>3</sub>	60 at room temperature	209

barriers are created at the interfaces between the noble metal and the metal oxide. Because noble metals have a large number of mobile electrons, electrons can easily redistribute themselves to counteract charge buildup near the heterojunction interface. The presence of a negative charge on the surface of the noble metal can attract electronegative species such as O<sub>2</sub> gas.<sup>219,220</sup> In the presence of the target gas, the height of the Schottky potential barrier changes, leading to a resistance change of the gas sensor, which contributes to the sensor signal.

Additionally, noble-metal catalysts have a chemical sensitization effect.<sup>188</sup> In chemical sensitization, noble metals (due to their catalytic activity) increase the adsorption of gases onto the sensor surface [Fig. 15(a)]. The gas molecules are first adsorbed on the surface of noble metals and then spill over to the surface of metal oxides. Spillover involves the transport of active species adsorbed

on a first surface onto another surface that is in intimate contact with the original adsorbing surface.<sup>221</sup> O<sub>2</sub> or target gases can be adsorbed on the surface of noble metals and be dissociated into chemisorbed mono atomic O, finally spilling over onto the surface of metal oxide. For example, Pd can easily dissociate H<sub>2</sub> gas into atomic H. Then, the atomic H species can be adsorbed onto the surface of the sensing material. Therefore, significantly more H atoms can react with the already adsorbed O species, resulting in an improved gas response, shorter response and recovery times, and higher selectivity of the gas sensor.<sup>222,223</sup> However, an excessive particle size reduces the surface area of the gas sensor and may significantly reduce the response of the gas sensor.<sup>224</sup> Because of the high catalytic activity of noble metals to specific gases, many highly selective NW gas sensors with noble-metal functionalization have been reported in the literature.<sup>225,226</sup>

In electronic sensitization, the change of the noble-metal state (metallic) to an oxidized state significantly affects the resistance of the gas sensor [Fig. 15(b)]. For example, Pd can be oxidized to PdO in oxidizing atmospheres, which causes a large resistance modulation via electronic sensitization mechanisms.<sup>219</sup> Similarly, in an air atmosphere, some noble metals, such as Ag and Pd, generally become partially oxidized. When they are exposed to reducing gases, their electronic properties and work functions change, leading to the resistance modulation of the gas sensor.<sup>70</sup> A similar type of change was observed in a H<sub>2</sub> gas atmosphere, where Pd transformed into PdH<sub>x</sub>, which is associated with a large resistance modulation.<sup>165</sup> Although noble-metal additives have proven to be very effective for improving the sensor performance, their high cost limits their applicability.<sup>227,228</sup>

Sensor poisoning by toxic gases is a major issue for practical applications, as it reduces the sensor lifetime. Poisoning refers to an irreversible change in the surface properties due to contaminations.<sup>229</sup> Generally, noble metals such as Pd can be poisoned by many organic and inorganic chemicals that contain S (H<sub>2</sub>S, SO<sub>2</sub>, thiols) or P. Sulfide compounds can be directly coordinated with Pd using two antibonding lone pairs. Therefore, the activity of a Pd catalyst can significantly decreased by sulfide.<sup>230</sup> This can be due to a decrease in the number of active sites or a change in their nature. Using filters or by recovery through thermal treatment (regeneration), poisoning can be reduced or avoided. The regeneration should be carried out in a way to remove all other poisoning elements while do not damage the sensor material.<sup>229</sup> Owing to their irreversible adsorption, the catalytic activity of noble metals exposed to a poison can be reduced to zero. The deactivation rate depends on the nature of the catalyst, the poison, and the diffusion

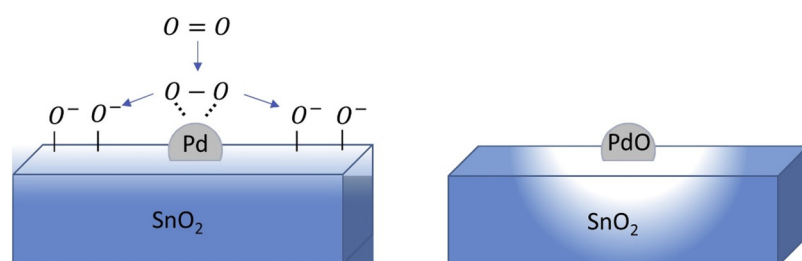


FIG. 15. (a) Chemical sensitization and (b) electronic sensitization effects of noble metals. Reproduced with permission from Walker *et al.*, Sens. Actuators B Chem. 286, 624–640 (2019). Copyright 2019 Elsevier.

and reaction under consideration. Thus, depending on the exact physical and chemical nature of the system, the slow nonselective poisoning to rapid highly selective poisoning can be observed.<sup>231</sup> Therefore, an alternative approach to increase the performance of NW gas sensors is the realization of heterojunctions.

Heterojunction formation is a very popular method for the fabrication of high-performance gas sensors. In heterojunctions (which can be n-n, n-p, or p-p), because the Fermi levels of the semiconducting materials are different, the electrons at the higher energies are transferred to unoccupied lower-energy states until the Fermi energies are equalized. Accordingly, a net positive charge and a net negative charge in the materials in contact are created. The flow of electrons continues until the negative charge increases the energy of the electrons to prevent the further flow of electrons.<sup>219</sup> Schematics of p-n and n-n junctions are shown in Fig. 16. Because of the band bending, a potential energy barrier is established at the interface. To cross the interface, electrons must overcome this potential energy barrier.

In heterojunction NWs, e.g., an n-type NW sensor in intimate contact with a p-type metal oxide, due to the transfer of electrons from the n-type NWs to the p-type material, the diameter of the charge-conduction channel inside the n-type NWs decreases, which leads to an increase in the air resistance. When the sensor is in an oxidizing gas atmosphere such as NO<sub>2</sub>, a low response can be expected, because there are not enough electrons in the n-type NWs to be withdrawn by NO<sub>2</sub> molecules. However, in the presence of a reducing gas, a significant change in the diameter of the charge-conduction channel occurs; thus, a high response is expected. This was confirmed by Na *et al.*<sup>233</sup> for a p-Cr<sub>2</sub>O<sub>3</sub>/n-ZnO NW gas sensor.

#### XIV. LOW-POWER CONSUMPTION STRATEGIES: LIGHT ACTIVATION AND SELF-HEATING OPERATION

##### A. Light activation

One of the major issues associated with the operating condition and stability of metal-oxide NWs is the relatively high working temperature, which is needed to enhance surface reactions to activate adsorbed O<sub>2</sub> and to enhance the reactivity with the target gas. Camagni *et al.*<sup>234</sup> reported a UV-enhanced sensing signal, and it was confirmed that UV light could improve the sensing performance at room temperature and low temperatures. Additionally, Law *et al.*<sup>235</sup> reported that UV illumination enhanced the response of NW gas sensors.

When a metal-oxide NW gas sensor is in a dark environment at room temperature, only a few O<sub>2</sub> molecules can be adsorbed on the surface of the gas sensor, and they are difficult to be desorbed. For the activation of the sensing layer, a minimum energy equal to the energy of the bandgap of the metal oxide is required. Illumination of the sensor with UV light having a photon energy equal to or higher than the bandgap of the metal-oxide NWs can cause excitation of electrons from the valence band to the conduction band. Consequently, a large number of UV-induced electron-hole pairs can be generated in the NWs.

Additionally, it has been reported that using photons with excessive energies—above the threshold of the bandgap—does not necessarily yield better responses, because with the increasing energy, a larger fraction of conduction electrons are lost due to inelastic scattering. Therefore, the maximum response can correspond to photons with an energy close to the bandgap of the metal

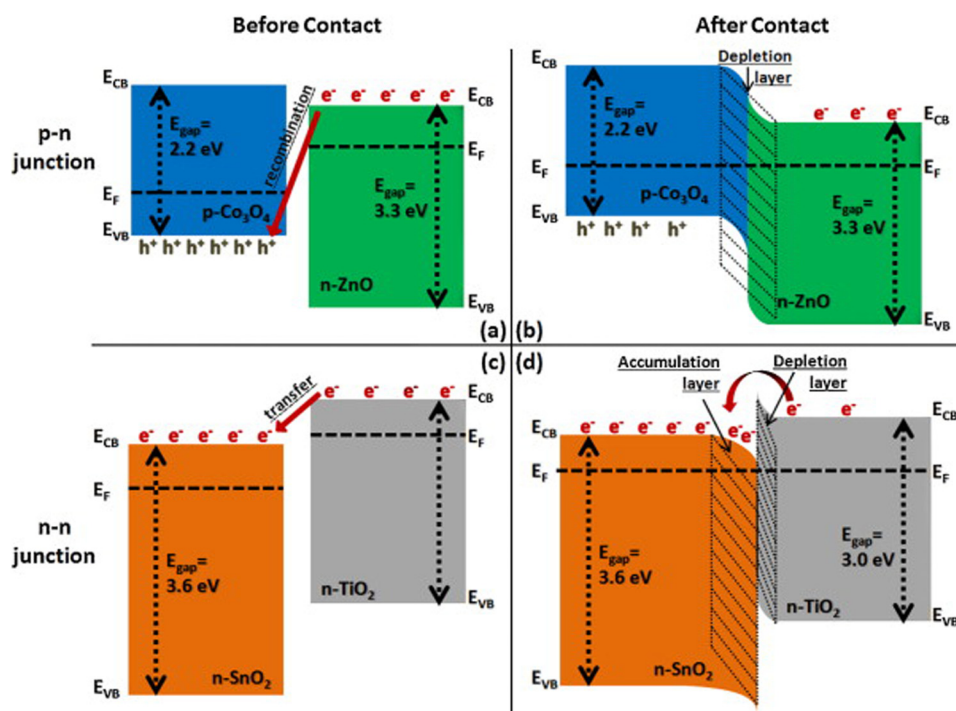


**FIG. 16.** (a) p-n junction before formation. (b) Depletion layer formed on both sides of the p-n junction due to electron-hole recombination. (c) n-n junction before formation. (d) Depletion layer and accumulation layer. Reproduced with permission from Miller *et al.*, *Sens. Actuators B Chem.* **204**, 250–272 (2014). Copyright 2019 Elsevier.

oxide.<sup>236</sup> The maximum wavelength of UV light that can be used for activation is expressed as follows:

$$\lambda_{\max} \leq hc/E_g, \quad (8)$$

where  $h$  represents Planck's constant ( $4.14 \times 10^{-15}$  eV s),  $c$  represents the velocity of light ( $3.00 \times 10^8$  m s<sup>-1</sup>), and  $E_g$  represents the bandgap.

UV illumination enhances the surface chemical activity by increasing the number of charge carriers in the conduction band. Thus, it increases the number of active sites on the surface. The target gas molecules can then be easily adsorbed and react with O atoms on the surface of the gas sensor. This significantly affects the layer conductivity due to the change in the number of electrons, allowing the gas concentration to be measured by monitoring the conductance change over time.<sup>237</sup>

Two mechanisms are proposed for the direct desorption of adsorbates upon exposure to UV radiation: (1) direct excitation of a binding electron to the conduction band and (2) recombination with a photogenerated hole in the valence band. As the photons irradiate the surface, the photoinduced holes/electrons interact with the adsorbed O<sub>2</sub>, leading to desorption of O ion species (photo-desorption) and the simultaneous interaction of the photoinduced electrons with O<sub>2</sub> in the gas phase. This phenomenon reaches a new equilibrium state in which the rates of arrival of the holes and electrons to the surface become equal. Interaction and recombination of a hole with a binding electron of the layer can also break the bond and provide an O atom that is able to diffuse to the crystal surface, react with O ions, form O<sub>2</sub>(g), and leave an O vacancy behind.<sup>237</sup>

Consider the cross section of a metal-oxide NW such as ZnO, as schematically described in Fig. 17. Because of the built-in electric field in air, under UV illumination, photogenerated holes on the surface react with adsorbed O species, causing their desorption. Simultaneously, photoinduced O species are created through the interaction between the O<sub>2</sub> molecules and the active photoelectrons. They are bound to the surface weakly compared with chemisorbed O species. In the target gas atmosphere, the change in the resistance of the ZnO sensor increases under UV activation. Therefore, the metal-oxide NW gas sensor exhibits a fast response-recovery time under UV light at a low sensing temperature.<sup>236</sup>

The pattern and intensity of the emitted UV light affect the flow of photons, thus influencing the performance and sensing characteristics, due to the change in the carrier density due to the photon interactions. Park *et al.*<sup>238</sup> reported that the response of ZnS-core/ZnO-shell NWs increased from 116% to 118% as the UV light intensity increased from 0 to 1.2 mW/cm<sup>2</sup>. A higher intensity of UV light may increase the number of electron-hole pairs, which significantly increases the charge-carrier concentration, resulting in room-temperature operation and a higher response of the gas sensor. Another method of power-consumption reduction is operation of the gas sensor in the self-heating mode.

In some cases, e.g., in sensor arrays, UV illumination cannot result in a high response, and a battery is required for operation. Generally, the working temperature of gas sensors is high, limiting their use in some places. However, when the number of sensors in a sensor array or a network is large, replacing individual batteries is a

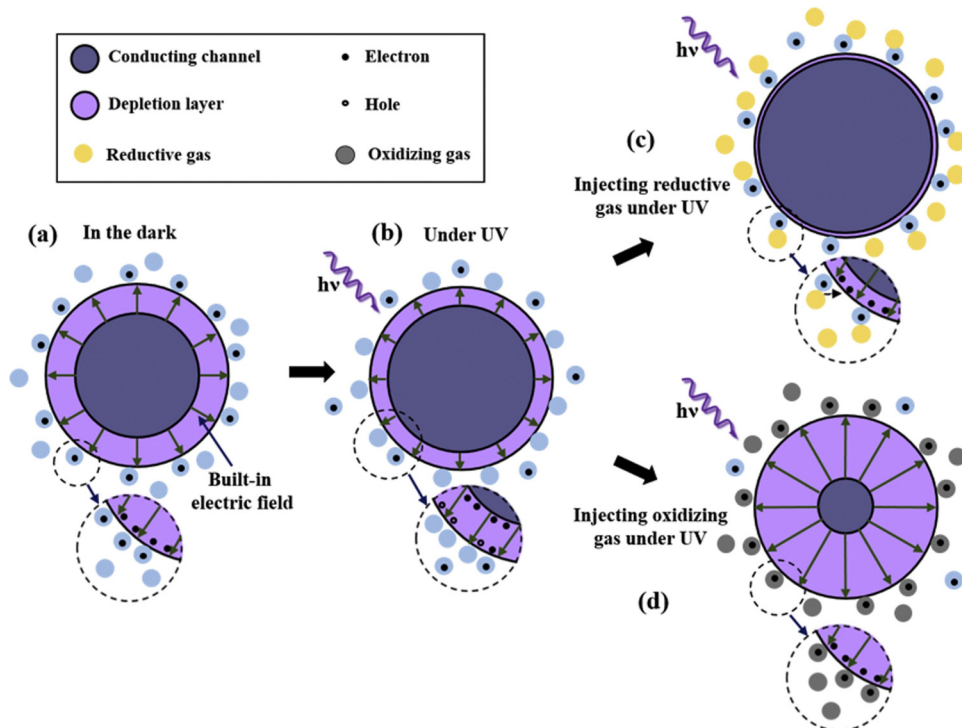


**FIG. 17.** Gas-sensing mechanism of ZnO (a) in air, (b) in air under UV light, (c) in a reducing gas under UV light, and (d) in an oxidizing gas under UV light. Reproduced with permission from Zhu and Zeng, *Sens. Actuators A Phys.* **267**, 242–261 (2017). Copyright 2019 Elsevier.



tedious and difficult task. Furthermore, the battery materials are potentially hazardous to human health. Therefore, novel approaches for reducing the power consumption of gas sensors are needed.<sup>239</sup> With the use of micromachining technology, the power consumption can be lower than 30–50 mW. Further reduction of the power consumption is possible with a self-heating strategy.<sup>229,240</sup>

## B. Self-heating operation

Self-powered electronic devices were introduced by Xu *et al.* using ZnO NWs. In this study, a voltage of 1.26 V was produced by ZnO NWs, which was sufficient to recharge an AA battery.<sup>241</sup> For the first time, Salehi applied an alternating-current bias to a self-heated SnO<sub>2</sub> gas sensor without external heating and demonstrated its successful operation for sensing.<sup>242</sup> Further studies revealed that metal-oxide NW gas sensors as well as metallic NWs<sup>243,244</sup> can operate in the self-heating mode, with a significant reduction of the power consumption (a few tens of microwatts). Prades *et al.*<sup>245</sup> reported the self-heated operation of SnO<sub>2</sub> NWs for NO<sub>2</sub> sensing with a power consumption of <20 μW, which was remarkably lower than 140 mW required for the external microheater.

The main advantages of NWs for self-heating compared with thin film- and thick film-based gas sensors are their small thermal capacitance and the significant reduction of thermal losses to the electrodes as well as the gas environment.<sup>240</sup> Self-heating operation has the following disadvantage: during the Joule heating, the steady-state temperature is sometimes not homogeneous along the NW length, which increases the response time of self-heated gas sensors.<sup>213</sup> In the self-heating mode, the small amount of power used to probe the sensor resistance is sufficient to reach the optimum temperature of the gas sensor (Fig. 18). Self-heating gas sensors not only eliminate the need for external heaters but also significantly reduce the power consumption.<sup>246</sup>

The working principle is based on Joule's Law, which can be expressed as follows:

$$Q = V^2/R, \quad (9)$$

where  $Q$  represents the dissipated power,  $V$  represents the voltage applied between the electrodes, and  $R$  represents the total resistance

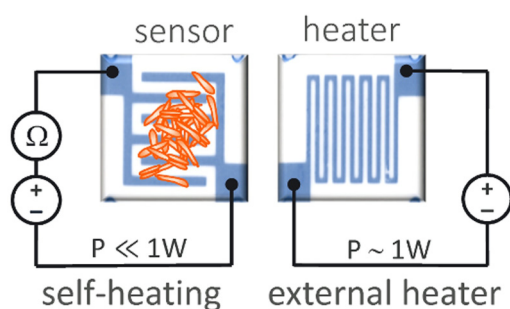


**FIG. 18.** Schematic of gas sensors operating in the self-heating and conventional modes. Reproduced with permission from Fàbrega *et al.*, *Sens. Actuators B Chem.* **256**, 797–811 (2018). Copyright 2019 Elsevier.

of the samples.<sup>247</sup> The figure of merit of self-heated gas sensors, which is called the efficient self-heating (ESH) coefficient, can be obtained as follows:

$$\text{ESH} = \Delta T/Q, \quad (10)$$

where  $\Delta T$  represents the temperature increase of the sensor when it is subjected to electrical power dissipation  $Q$ . For ESH values of >1, an increase of several Kelvin per microwatt can be resulted. For realization of hundreds of Kelvin, power consumptions well below the milliwatt regime are attainable.<sup>248</sup> The increment of the temperature is inversely proportional to the cross section of the 1D nanostructure being heated. In the case of cylindrical NWs, this relationship can be expressed as follows:

$$\Delta T = \frac{1}{r_{nw}^2}, \quad (11)$$

where  $r_{nw}$  represents the radius of the NWs (or, more generally for a 1D material, any characteristic dimension of the transversal confinement). Accordingly, because the temperature rise is inversely proportional to the squared radius of the NWs, a smaller diameter of NWs is better for self-heating. Additionally, the thermal conductivity of NWs should be as high as possible, and the thermal losses of all elements in contact with the self-heated NWs should be reduced.<sup>246</sup>

For self-heating gas sensors, it is generally accepted that multiple NWs have better performance than a single NW. In the case of multiple NWs, because there are many NWs between the electrodes, the risk of sensor damage due to failure of an NW decreases. Moreover, the conductivity range of multiple-NW sensors permits the application of far easier and less expensive electronic devices for operation of the gas sensor. However, in a single-NW gas sensor, the gas diffusion processes can be minimized, which can reduce the response and recovery times.<sup>248,249</sup>

For self-heated gas sensors, the following points are important: (i) because the temperature rise is inversely proportional to the squared radius of the NWs, a smaller diameter of the NWs is better for self-heating; (ii) the thermal conductivity of NWs should be as high as possible; and (iii) the thermal losses of all elements in contact with the self-heated NWs should be reduced.<sup>246</sup>

Kim *et al.*<sup>250</sup> reported Pt-functionalized SnO<sub>2</sub>-ZnO C-S NWs with a shell thickness of 10–85 nm operating in the self-heating mode for gas sensing. Generally, in self-heating studies, thermographs similar to those in Fig. 19 are obtained to confirm the self-heating effect. The measured temperature increased with increasing shell thickness. There were three sources of Joule heating in the C-S NWs. First, because electrons passed through the ZnO grains, Joule heating occurred inside the ZnO grains [Fig. 20(a)]. Second, the ZnO grain boundaries acted as another source of Joule heating [Fig. 20(b)]. Third, because the ZnO NWs were in intimate contact, Joule heating was caused by the electrical currents flowing through the ZnO-ZnO homojunctions [Fig. 20(c)]. Increasing the shell thickness increased the diameter of the C-S NWs and the probability of contact between NWs, which led to a higher temperature. This resulted in a higher C<sub>7</sub>H<sub>8</sub> response of the sensor with an 85-nm-thick shell.



Operating voltage	SnO <sub>2</sub> -ZnO C-S NWs ZnO shell thickness: 10 nm		SnO <sub>2</sub> -ZnO C-S NWs ZnO shell thickness: 30 nm		SnO <sub>2</sub> -ZnO C-S NWs ZnO shell thickness: 85 nm	
	Thermographic image	Measured Temp.	Thermographic image	Measured Temp.	Thermographic image	Measured Temp.
0 V		24.6 °C		24.7 °C		25.2 °C
1 V		24.4 °C		24.7 °C		25.2 °C
3 V		24.3 °C		24.6 °C		25.7 °C
5 V		23.8 °C		25.0 °C		28.5 °C
10 V		23.7 °C		27.3 °C		43.3 °C
20 V		30.3 °C		53.8 °C		92.4 °C

**FIG. 19.** Thermographs of Pt-functionalized SnO<sub>2</sub>-ZnO C-S NW sensors at different shell thicknesses and applied voltages. Reproduced with permission from Sens. Actuators B Chem. **251**, 781–794 (2017). Copyright 2019 Elsevier.

These results were confirmed by another study where a novel self-heated CO gas sensor using Au-functionalized networked SnO<sub>2</sub>-ZnO C-S NWs was demonstrated.<sup>251</sup> The three sources of Joule heating in the SnO<sub>2</sub>-ZnO C-S NWs were the resistance inside the ZnO grains, the resistance at grain boundaries, and the resistance in the ZnO-ZnO homojunctions. By increasing the ZnO shell thickness, the response was increased. The power consumption at 3 and 20 V was 11.3 nW and 8.3 μW, respectively. Increasing the applied voltage enhanced the sensing response due to the self-heating effect within the sensor, and the sensor exhibited good performance without an external heater. In a sensor with an optimal ZnO shell thickness of 80 nm, the responses for 50-ppm CO were 1.17 and 1.62 at 3 and 20 V, respectively. For the optimized ZnO shell, the catalytic effect of Au and the Joule effect contributed to the high response of the gas sensor to CO.<sup>251</sup>

## XV. METAL-OXIDE NWs IN ELECTRONIC-NOSE (E-NOSE) SYSTEM

The human nose can be used to measure the quality of food, drinks, perfumes, cosmetics, and chemical products. However, smelling some substances can be harmful to physical and mental health or cause fatigue. An e-nose is an instrument that combines

gas-sensor arrays and pattern-analysis techniques for the detection, identification, and quantification of gases. The multivariate response of an array of chemical gas sensors with broad and partially overlapping selectivity can be utilized as an “electronic fingerprint” to characterize a wide range of odors or gases via pattern recognition.<sup>252</sup> E-nose devices are composed of three main elements: (i) a sampling system, (ii) a detection system, and (iii) data-processing and pattern-recognition algorithms.<sup>253</sup> Data-processing techniques used in postprocessing of pattern-recognition routines include principal component analysis, linear discriminate analysis, partial least squares, functional discriminate analysis, cluster analysis, fuzzy logic, and artificial neural networks, such as probabilistic neural networks.<sup>254</sup>

The working principle of e-nose systems is shown in Fig. 21. The odor/gas molecules are drawn into the e-nose and induce a reversible physical and/or chemical change in the sensing material, which changes the electrical resistance. Each “cell” in the array can behave as a receptor by responding to different odors to varying degrees. These changes are transduced into electrical signals, which are preprocessed and conditioned before identification by a pattern-recognition system.<sup>255</sup>

The e-nose detection system has a significantly lower price than chromatography and mass-spectrometry systems. Additionally, it is portable and has a fast response.<sup>255</sup> However, for further application

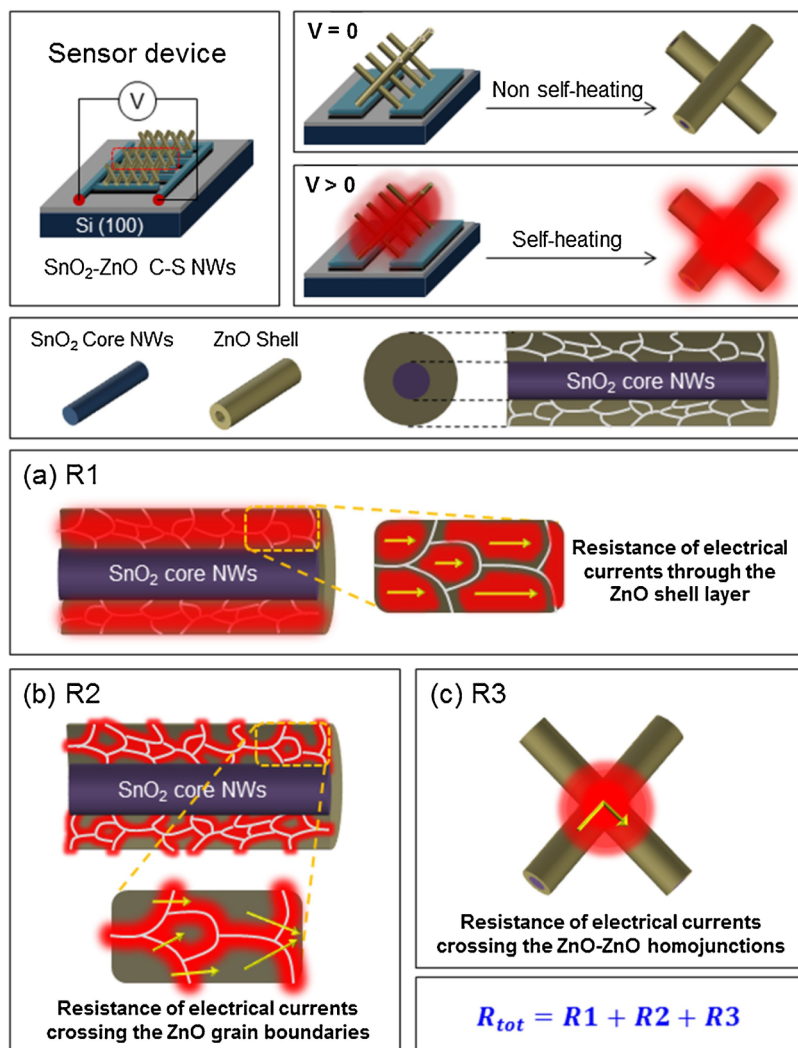


**FIG. 20.** Schematic of self-heated gas sensors and (a)–(c) sources of resistance in the C-S NWs. Reproduced with permission from Kim *et al.*, *Sens. Actuators B Chem.* **251**, 781–794 (2017). Copyright 2019 Elsevier.

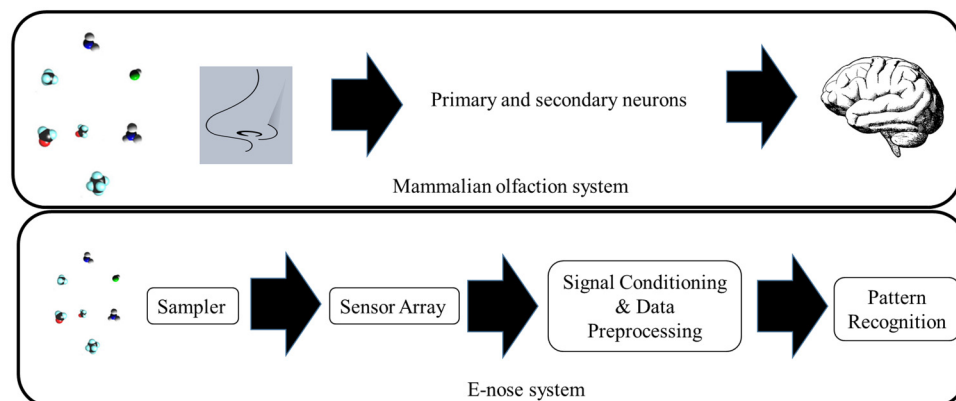


**FIG. 21.** Comparison of the mammalian olfactory system and the e-nose system. Adapted from Arshak *et al.*, *Sens. Rev.* **24**(2), 181–198 (2004). Copyright 2004 Emerald Publishing Ltd.

of e-noses, their robustness, selectivity, and reproducibility should be enhanced. Moreover, the e-noses should use appropriate pattern-recognition algorithms that can cope with complex signal analysis. Nonetheless, the use of e-noses is rapidly expanding in different areas,<sup>255</sup> such as quality control in the food industry, environmental monitoring, public health, detection of explosives, and spaceflight applications.<sup>256</sup>

Metal oxide-based e-nose systems generally operate at high temperatures (300–550 °C); thus, they consume a large amount of energy for operation. Compared with conducting polymer (CP)-based systems, they have higher sensitivity, higher stability, and shorter response and recovery times but are susceptible to S and weak-acid poisoning and sensitive to high humidity.<sup>257</sup> For e-nose applications, the selection of the materials is important for achieving good discrimination for the specific application. However, the selectivity is still a major challenge.<sup>254</sup>

With the further development of NW gas sensors, large arrays of macroscopic individual gas sensors will be replaced with an e-nose embodied in a single device that integrates the sensing and signal-processing functions in one chip. The e-nose can be comprised of an array of NW gas sensors (e.g., NW-based resistors and field-effect sensors). Therefore, the selectivity and stability of the gas-sensor devices can be improved.<sup>258</sup> Baik *et al.*<sup>259</sup> synthesized SnO<sub>2</sub> NWs functionalized with different noble metals for e-nose application. The sensors could distinguish three reducing gases (H<sub>2</sub>, CO, and ethylene) and were able to do so unequivocally when the data were classified using linear discriminant analysis. The discriminating ability of this e-nose design was not impacted by the lengths or diameters of the NWs used. Sysoev *et al.*<sup>260</sup> synthesized SnO<sub>2</sub> NWs, SnO<sub>2</sub>:Ni NWs, and TiO<sub>2</sub> and In<sub>2</sub>O<sub>3</sub> mesoscopic whiskers and assembled them as an array of chemiresistors on a single chip. The responses to low concentrations of H<sub>2</sub> and CO mixed with O<sub>2</sub> were compared. The differences of the gas responses of the NWs were mainly governed by the ratio of the diameter of the nanostructure to its Debye length. Additionally, it was reported that discrimination between H<sub>2</sub> and CO could be achieved using the e-nose system through an analysis of the responses from the three-NW array.

## XVI. CONCLUSIONS AND OUTLOOK

The next generation of sensing devices will require significant enhancements in sensitivity and selectivity to satisfy demands in a variety of fields. Metal-oxide sensors based on NWs take advantage of fundamental nanoeffects to satisfy these requirements. NWs are novel lightweight, low-dimensional materials that have exceptional mechanical, electrical, thermal, and multifunctional properties. Their small size and very high aspect ratio are particularly useful for electrical sensors. In this tutorial article, different aspects of metal-oxide NW-based gas sensors were reviewed, including their synthesis routes and their sensing parameters and mechanisms. Single-NW gas sensors can offer relatively high sensing performance and low LODs owing to their large surface area, excellent crystallinity, and small diameter. However, their implantation in practical devices and fabrication remain difficult. Because they exhibit larger amounts of homojunctions and heterojunctions, multiple NWs and

branched NWs offer higher sensing responses. Additionally, they can be easily synthesized and implemented, e.g., by using VLS growth methods. The surface functionalization of the NWs with noble metals such as Pt, Pd, or Au allows the sensitivity and selectivity of these sensors to be enhanced. In heterojunction NWs, due to the presence of two materials with different work functions, the large modulation of the resistance at the interfaces can significantly increase the sensing response. In C-S NWs, there is often an optimal shell thickness yielding the highest gas-sensing response. With UV irradiation, gas sensors can operate at a lower temperature, reducing their power consumption significantly. Another method for reducing the power consumption is the self-heating strategy, which allows for the preparation of NW gas sensors with extremely low power demands. MOF nanomaterials can be used for the fabrication of highly selective gas sensors, as these porous structures act as selective membranes, allowing certain gas molecules to pass through their small pores, which results in a high selectivity. According to this tutorial, NWs have potential for high-performance, low-power consumption, and low-cost gas sensors. In this regard, the optimal amounts of noble metals, shell thickness, selection of an appropriate MOF membrane, sensing temperature, and sensing layer are important factors. The value of sensing devices lies in their sensitivity, selectivity, stability, and detection-limit range. NW-modified sensor electrodes enhance all these parameters. Thus, NW-based sensors are inherently useful, as long as the sensing device platforms are optimally engineered such that most of the NW surface can be integrated. These additional benefits allow the development of small and multifunctional sensors. It is expected that in the near future, more sensitive, selective, and stable gas sensors with metal oxide-based NW structures will be developed and that such NW sensors will become common in research and in the market.

## ACKNOWLEDGMENTS

This research was supported by Basic Science Research Program through the National Research Foundation of Korea (NRF) funded by the Ministry of Education (2016R1A6A1A03013422). This work was supported by the National Research Foundation of Korea (NRF) grant funded by the Korea government (MSIT) (2019R1A2C1006193).

## REFERENCES

- <sup>1</sup>Y. Fu, Y. Nie, Y. Zhao, P. Wang, L. Xing, Y. Zhang, and X. Xue, *ACS Appl. Mater. Interfaces* **7**, 10482–10490 (2015).
- <sup>2</sup>S. J. Patil, A. V. Patil, C. G. Dighavkar, K. S. Thakare, R. Y. Borase, S. J. Nandore, N. G. Deshpande, and R. R. Ahire, *Front. Mater. Sci.* **9**, 14–37 (2015).
- <sup>3</sup>A. Baroutaji, T. Wilberforce, M. Ramadan, and A. G. Olabi, *Renew. Sustain. Energy Rev.* **106**, 31–40 (2019).
- <sup>4</sup>T. Hübert, L. Boon-Brett, G. Black, and U. Banach, *Sens. Actuators B Chem.* **157**, 329–352 (2011).
- <sup>5</sup>S.-C. Xu, Y.-M. Miao, C. Gao, R.-Y. Long, H. Chen, B. Zhao, and S.-X. Wang, *J. Clean. Prod.* **208**, 340–352 (2019).
- <sup>6</sup>T. Ahmad, S. M. Majhi, X. Zhang, T. M. Swager, and K. N. Salama, *Adv. Colloid Interface Sci.* **270**, 1–27 (2019).
- <sup>7</sup>A. Luengas, A. Barona, C. Hort, G. Gallastegui, V. Platel, and A. Elias, *Rev. Environ. Sci. Bio.* **14**, 499–522 (2015).

- <sup>8</sup>A. J. Bandari and S. Nasirian, *J. Mater. Sci. Mater. Electronics* **30**(11), 10073–10081 (2019).
- <sup>9</sup>T.-Y. Wong, *J. Food Drug Anal.* **25**, 235–244 (2017).
- <sup>10</sup>M. Kuniavsky, Y. Bechor, M. Leitman, and S. Efrati, *Intensive Crit. Care Nurs.* **47**, 85–88 (2018).
- <sup>11</sup>K. Thorsteinsson, R. N. Mortensen, C. Torp-Pedersen, B. Kjærgaard, and J. J. Andreasen, *PLoS One* **14**, e0210767 (2019).
- <sup>12</sup>S. M. Hosseineinejad, H. Aminiahdashti, I. Goli Khatir, S. K. Ghasempouri, A. Jabbari, and M. Khandashpour, *J. Forensic Leg. Med.* **53**, 87–96 (2018).
- <sup>13</sup>S. Hammond and J. A. Phillips, *Workplace Health Saf.* **67**, 47–48 (2019).
- <sup>14</sup>J. Garg, P. Krishnamoorthy, C. Palaniswamy, S. Khera, H. Ahmad, D. Jain, W. S. Aronow, and W. H. Frishman, *Am. J. Ther.* **25**, e339–e348 (2018).
- <sup>15</sup>R. Kumar, O. Al-Dossary, G. Kumar, and A. Umar, *Nanomicro Lett.* **7**, 97–120 (2015).
- <sup>16</sup>S. W. Lee, W. Lee, Y. Hong, G. Lee, and D. S. Yoon, *Sens. Actuators B Chem.* **255**, 1788–1804 (2018).
- <sup>17</sup>S. K. Pandey, K.-H. Kim, and K.-T. Tang, *Trends Anal. Chem.* **32**, 87–99 (2012).
- <sup>18</sup>A. Mirzaei, S. S. Kim, and H. W. Kim, *J. Hazard. Mater.* **357**, 314–331 (2018).
- <sup>19</sup>M. Greabu, A. Totan, D. Miricescu, R. Radulescu, J. Virlan, and B. Calenic, *Antioxidants* **5**, 3 (2016).
- <sup>20</sup>M. S. Kamal, S. A. Razzak, and M. M. Hossain, *Atmos. Environ.* **140**, 117–134 (2016).
- <sup>21</sup>A. Mirzaei, S. G. Leonardi, and G. Neri, *Ceram. Int.* **42**, 15119–15141 (2016).
- <sup>22</sup>H. Huang, Y. Xu, Q. Feng, and D. Y. C. Leung, *Catal. Sci. Technol.* **5**, 2649–2669 (2015).
- <sup>23</sup>A. Mirzaei, J.-H. Kim, H. W. Kim, and S. S. Kim, *J. Mater. Chem. C* **6**, 4342–4370 (2018).
- <sup>24</sup>F. Ren, L. Gao, Y. Yuan, Y. Zhang, A. Alqarni, O. M. Al-Dossary, and J. Xu, *Sens. Actuators B Chem.* **223**, 914–920 (2016).
- <sup>25</sup>K. Kawamura, K. Kerman, M. Fujihara, N. Nagatani, T. Hashiba, and E. Tamiya, *Sens. Actuators B Chem.* **105**, 495–501 (2005).
- <sup>26</sup>A. Majid and N. Kruspe, *Curr. Biol.* **28**, 409–413.e2 (2018).
- <sup>27</sup>C. Linster and O. Escanilla, *Brain Res.* **1709**, 33–38 (2019).
- <sup>28</sup>N. Aguilar Martínez, G. Aguado Carrillo, P. E. Saucedo Alvarado, C. A. Mendoza García, A. L. Velasco Monroy, and F. Velasco Campos, *Rev. Med. Hosp. Gen. Méx.* **81**, 268–275 (2018).
- <sup>29</sup>X. Bao, E. Gjorgieva, L. K. Shanahan, J. D. Howard, T. Kahnt, and J. A. Gottfried, *Neuron* **102**, 1066–1075.e5 (2019).
- <sup>30</sup>V. Grabe and S. Sachse, *Biosystems* **164**, 94–101 (2018).
- <sup>31</sup>J. P. McGann, *Science* **356**, eaam7263 (2017).
- <sup>32</sup>Y. Bu, S. Er, J. W. H. Niemantsverdriet, and H. O. A. Fredriksson, *J. Catal.* **357**, 176–187 (2018).
- <sup>33</sup>A.-L. Moriaux, R. Vallon, B. Parvitte, V. Zeninari, G. Liger-Belair, and C. Cilindre, *Food Chem.* **264**, 255–262 (2018).
- <sup>34</sup>C. Becker, M. A. Jochmann, and T. C. Schmidt, *Trends Anal. Chem.* **110**, 143–149 (2019).
- <sup>35</sup>M. C. M. M. Souza, A. Grieco, N. C. Frateschi, and Y. Fainman, *Nat. Commun.* **9**, 665 (2018).
- <sup>36</sup>M. Meyyappan, *Small* **12**, 2118–2129 (2016).
- <sup>37</sup>I. Simon, N. Bársan, M. Bauer, and U. Weimar, *Sens. Actuators B Chem.* **73**, 1–26 (2001).
- <sup>38</sup>A. Hulanicki, S. Glab, and F. Ingman, *Pure Appl. Chem.* **63**, 1247–1250 (1991).
- <sup>39</sup>B. Liu, X. Chen, H. Cai, A. M. Mohammad, X. Tian, L. Tao, Y. Yang, and T. Ren, *J. Semicond.* **37**, 021001 (2016).
- <sup>40</sup>T. Liu, X. Zhang, L. Yuan, and J. Yu, *Solid State Ionics* **283**, 91–102 (2015).
- <sup>41</sup>C. Schwandt, R. V. Kumar, and M. P. Hills, *Sens. Actuators B Chem.* **265**, 27–34 (2018).
- <sup>42</sup>Y. Wu, B. Yao, C. Yu, and Y. Rao, *Sensors* **18**, 941 (2018).
- <sup>43</sup>H.-E. Joe, H. Yun, S.-H. Jo, M. B. G. Jun, and B.-K. Min, *Int. J. Precis. Eng. Manuf.* **5**, 173–191 (2018).
- <sup>44</sup>A. Mirzaei, J.-H. Kim, H. W. Kim, and S. S. Kim, *Appl. Sci.* **9**, 1775 (2019).
- <sup>45</sup>M. Chen, L. Zou, Z. Zhang, J. Shen, D. Li, Q. Zong, G. Gao, G. Wu, J. Shen, and Z. Zhang, *Carbon* **130**, 281–287 (2018).
- <sup>46</sup>T. Addabbo, A. Fort, M. Mugnaini, V. Vignoli, A. Baldi, and M. Bruzzi, *IEEE Trans. Instrum. Meas.* **67**, 722–730 (2018).
- <sup>47</sup>A. S. Pranti, D. Loof, S. Kunz, M. Bäumer, and W. Lang, *Proceedings* **2**, 927 (2018).
- <sup>48</sup>A. Harley-Trochimczyk, T. Pham, J. Chang, E. Chen, M. A. Worsley, A. Zettl, W. Mickelson, and R. Maboudian, *Adv. Funct. Mater.* **26**, 433–439 (2016).
- <sup>49</sup>P. Tardy, J.-R. Coulon, C. Lucat, and F. Menil, *Sens. Actuators B Chem.* **98**, 63–68 (2004).
- <sup>50</sup>C. Tsamis, A. G. Nassiopoulou, and A. Tserepi, *Sens. Actuators B Chem.* **95**, 78–82 (2003).
- <sup>51</sup>X. Cao, Z. Zhang, and X. Zhang, *Sens. Actuators B Chem.* **99**, 30–35 (2004).
- <sup>52</sup>A. Mirzaei and G. Neri, *Sens. Actuators B Chem.* **237**, 749–775 (2016).
- <sup>53</sup>Z. U. Abideen, J.-H. Kim, J.-H. Lee, J.-Y. Kim, A. Mirzaei, H. W. Kim, and S. S. Kim, *J. Korean Ceram. Soc.* **54**, 366–379 (2017).
- <sup>54</sup>K. C. Sekhar and S. S. C. Rao, *Indian J. Anaesth.* **58**, 350–352 (2014).
- <sup>55</sup>C. Pollock, *J. Avian Med. Surg.* **30**, 386–391 (2016).
- <sup>56</sup>W. H. Brattain and J. Bardeen, *Bell Syst. Tech. J.* **32**, 1–41 (1953).
- <sup>57</sup>G. Heiland, *Z. Phys.* **138**, 459–464 (1954).
- <sup>58</sup>T. Seiyama, A. Kato, K. Fujiishi, and M. Nagatani, *Anal. Chem.* **34**, 1502–1503 (1962).
- <sup>59</sup>N. Taguchi, Japanese patent 23 (October 1962).
- <sup>60</sup>K. Ihokura and J. Watson, *The Stannic Oxide Gas Sensor Principles and Applications* (CRC Press, Boca Raton, FL, 2017).
- <sup>61</sup>C. Wang, L. Yin, L. Zhang, D. Xiang, and R. Gao, *Sensors* **10**, 2088–2106 (2010).
- <sup>62</sup>B. Zhang and P.-X. Gao, *Front. Mater.* **6**, 55 (2019).
- <sup>63</sup>M. Drobek, J.-H. Kim, M. Bechelany, C. Vallicari, A. Julbe, and S. S. Kim, *ACS Appl. Mater. Interfaces* **8**, 8323–8328 (2016).
- <sup>64</sup>H.-R. Francisco, J. D. Prades, and J. R. Morante, *Sens. Mater.* **21**, 219–227 (2009).
- <sup>65</sup>A. Šutka and K. A. Gross, *Sens. Actuators B Chem.* **222**, 95–105 (2016).
- <sup>66</sup>E. Joanni, R. Savu, P. R. Bueno, E. Longo, and J. A. Varela, *Appl. Phys. Lett.* **92**, 132110 (2008).
- <sup>67</sup>G. Korotcenkov, *Mater. Sci. Eng.* **139**, 1–23 (2007).
- <sup>68</sup>H.-J. Kim and J.-H. Lee, *Sens. Actuators B Chem.* **192**, 607–627 (2014).
- <sup>69</sup>N. S. Ramgir, Y. Yang, and M. Zacharias, *Small* **6**, 1705–1722 (2010).
- <sup>70</sup>N. Yamazoe, G. Sakai, and K. Shimano, *Catal. Surv. Asia* **7**, 63–75 (2003).
- <sup>71</sup>M. Hübner, C. E. Simion, A. Tomescu-Stănoiu, S. Pokhrel, N. Bársan, and U. Weimar, *Sens. Actuators B Chem.* **153**, 347–353 (2011).
- <sup>72</sup>X. Gao and T. Zhang, *Sens. Actuators B Chem.* **277**, 604–633 (2018).
- <sup>73</sup>S. Park, G.-J. Sun, H. Kheel, W. I. Lee, S. Lee, S.-B. Choi, and C. Lee, *Sens. Actuators B Chem.* **227**, 591–599 (2016).
- <sup>74</sup>G. Neri, *Chemosensors* **3**, 1–20 (2015).
- <sup>75</sup>P. Mohankumar, J. Ajayan, R. Yasodharan, P. Devendran, and R. Sambasivam, *Measurement* **140**, 305–322 (2019).
- <sup>76</sup>C. Di Natale, R. Paolesse, E. Martinelli, and R. Capuano, *Anal. Chim. Acta* **824**, 1–17 (2014).
- <sup>77</sup>M. Gardon and J. M. Guilemany, *J. Mater. Sci. Mater. Electron.* **24**, 1410–1421 (2013).
- <sup>78</sup>A. Mashir and R. A. Dweik, *Adv. Powder Technol.* **20**, 420–425 (2009).
- <sup>79</sup>G. Li, Z. Cheng, Q. Xiang, L. Yan, X. Wang, and J. Xu, *Sens. Actuators B Chem.* **283**, 590–601 (2019).
- <sup>80</sup>N. Bársan, D. Koziej, and U. Weimar, *Sens. Actuators B Chem.* **121**, 18–35 (2007).
- <sup>81</sup>N. Bársan and U. Weimar, *J. Electroceram.* **7**, 143–167 (2001).
- <sup>82</sup>A. Kolmakov and M. Moskovits, *Annu. Rev. Mater. Res.* **34**, 151–180 (2004).
- <sup>83</sup>L. Y. Kupriyanov, *Semiconductor Sensors in Physico-Chemical Studies*, 1st ed. (Elsevier, Amsterdam, 1996).
- <sup>84</sup>D. E. Willimas and K. F. E. Pratt, *Sens. Actuators B Chem.* **70**, 214–221 (2000).
- <sup>85</sup>N. Kazemi, B. Hashemi, and A. Mirzaei, *Process Appl. Ceram.* **10**, 97–105 (2016).



- <sup>86</sup>K. Arshak and I. Gaidan, *Mater. Sci. Eng.* **118**, 44–49 (2005).
- <sup>87</sup>S. M. Kim, H. J. Kim, H. J. Jung, J.-Y. Park, T. J. Seok, Y.-H. Choa, T. J. Park, and S. W. Lee, *Adv. Funct. Mater.* **29**, 1970039 (2019).
- <sup>88</sup>A. Mirzaei, B. Hashemi, and K. Janghorban, *J. Mater. Sci. Mater. Electron.* **27**, 3109–3144 (2016).
- <sup>89</sup>J.-H. Lee, “Technological realization of semiconducting metal oxide-based gas sensors,” in *Gas Sensors Based on Conducting Metal Oxides* (Elsevier, New York, 2019), pp. 167–216.
- <sup>90</sup>M. Tiemann, *Chem. Eur. J.* **13**, 8376–8388 (2007).
- <sup>91</sup>G. F. Fine, L. M. Cavanagh, A. Afonja, and R. Binions, *Sensors* **10**, 5469–5502 (2010).
- <sup>92</sup>A. Tsuruta, T. Itoh, M. Mikami, Y. Kinemuchi, I. Terasaki, N. Murayama, and W. Shin, *Materials* **11**, 981 (2018).
- <sup>93</sup>P. Rong, S. Ren, and Q. Yu, *Crit. Rev. Anal. Chem.* **49**, 336–349 (2019).
- <sup>94</sup>T. Wang, Y. Guo, P. Wan, H. Zhang, X. Chen, and X. Sun, *Small* **12**, 3748–3756 (2016).
- <sup>95</sup>M. Alvarado, E. Navarrete, A. Romero, J. L. Ramírez, and E. Llobet, *Sensors* **18**, 999 (2018).
- <sup>96</sup>H. Ma, L. Yu, X. Yuan, Y. Li, C. Li, M. Yin, and X. Fan, *J. Alloys Compd.* **782**, 1121–1126 (2019).
- <sup>97</sup>Y. Deng, *Semiconducting Metal Oxides for Gas Sensing* (Springer, New York, 2019).
- <sup>98</sup>A. K. Basu, P. S. Chauhan, M. Awasthi, and S. Bhattacharya, *Appl. Surf. Sci.* **465**, 56–66 (2019).
- <sup>99</sup>A. Gurlo, N. Barson, and U. Weimar, in *Oxides: Chemistry and Applications*, edited by J. L. G. Fierro (CRC Press, 2005).
- <sup>100</sup>G. Korotcenkov and B. K. Cho, *Sens. Actuators B Chem.* **244**, 182–210 (2017).
- <sup>101</sup>G. Korotcenkov and B. K. Cho, *Sens. Actuators B Chem.* **188**, 709–728 (2013).
- <sup>102</sup>S. R. Morrison, *Sens. Actuators* **12**, 425–440 (1987).
- <sup>103</sup>H. Tian, H. Fan, M. Li, and L. Ma, *ACS Sens.* **1**, 243–250 (2016).
- <sup>104</sup>B. Chen, S. Xiang, and G. Qian, *Acc. Chem. Res.* **43**, 1115–1124 (2010).
- <sup>105</sup>Y. Cui, B. Li, H. He, W. Zhou, B. Chen, and G. Qian, *Acc. Chem. Res.* **49**, 483–493 (2016).
- <sup>106</sup>T. Zhou, Y. Sang, X. Wang, C. Wu, D. Zeng, and C. Xie, *Sens. Actuators B Chem.* **258**, 1099–1106 (2018).
- <sup>107</sup>M. Weber, O. Graniel, S. Balme, P. Miele, and M. Bechelany, *Nanomaterials* **9**(11), 1552 (2019).
- <sup>108</sup>M. Weber, J.-H. Kim, J.-H. Lee, J.-Y. Kim, I. Iatsunskyi, E. Coy, M. Drogbek, A. Julbe, M. Bechelany, and S. S. Kim, *ACS Appl. Mater. Interfaces* **10**, 34765–34773 (2018).
- <sup>109</sup>A. K. Srivastava, *Sens. Actuators B Chem.* **96**, 24–37 (2003).
- <sup>110</sup>X. Liu, S. Cheng, H. Liu, S. Hu, D. Zhang, and H. Ning, *Sensors* **12**, 9635–9665 (2012).
- <sup>111</sup>A. B. Gadkari, T. J. Shinde, and P. N. Vasambekar, *IEEE Sens. J.* **11**, 849–861 (2011).
- <sup>112</sup>N. Wu, B. Wang, C. Han, Q. Tian, C. Wu, X. Zhang, L. Sun, and Y. Wang, *J. Mater. Chem. C* **7**, 7299–7307 (2019).
- <sup>113</sup>A. K. Nayak, R. Ghosh, S. Santra, P. K. Guha, and D. Pradhan, *Nanoscale* **7**, 12460–12473 (2015).
- <sup>114</sup>J. Li, Y. Lu, Q. Ye, M. Cinke, J. Han, and M. Meyyappan, *Nano Lett.* **3**, 929–933 (2003).
- <sup>115</sup>M. Bonyani, J. K. Lee, G.-J. Sun, S. Lee, T. Ko, and C. Lee, *Thin Solid Films* **636**, 257–266 (2017).
- <sup>116</sup>D. R. Patil, L. A. Patil, and P. P. Patil, *Sens. Actuators B Chem.* **126**, 368–374 (2007).
- <sup>117</sup>A. McLaren, T. Valdes-Solis, G. Li, and S. C. Tsang, *J. Am. Chem. Soc.* **131**, 12540–12541 (2009).
- <sup>118</sup>Y. H. Navale, S. T. Navale, F. J. Stadler, N. S. Ramgir, and V. B. Patil, *Ceram. Int.* **45**, 1513–1522 (2019).
- <sup>119</sup>J. Lee, S.-H. Lee, S.-Y. Bak, Y. Kim, K. Woo, S. Lee, Y. Lim, and M. Yi, *Sensors* **19**, 1903 (2019).
- <sup>120</sup>N. V. Hoang, C. M. Hung, N. D. Hoa, N. V. Duy, I. Park, and N. V. Hieu, *Sens. Actuators B Chem.* **282**, 876–884 (2019).
- <sup>121</sup>K. Wang, W. Wei, Z. Lou, H. Zhang, and L. Wang, *Appl. Surf. Sci.* **479**, 209–215 (2019).
- <sup>122</sup>X. Zhang, D. Song, Q. Liu, R. Chen, J. Hou, J. Liu, H. Zhang, J. Yu, P. Liu, and J. Wang, *J. Mater. Chem. C* **7**, 7219–7229 (2019).
- <sup>123</sup>I. Kortidis, H. C. Swart, S. S. Ray, and D. E. Motaung, *Sens. Actuators B Chem.* **285**, 92–107 (2019).
- <sup>124</sup>F. Loghini, A. Abdellah, A. Falco, M. Becherer, P. Lugli, and A. Rivadeneyra, *Measurement* **136**, 323–325 (2019).
- <sup>125</sup>Y. Seekaew, A. Wisitsoraat, D. Phokharatkul, and C. Wongchoosuk, *Sens. Actuators B Chem.* **279**, 69–78 (2019).
- <sup>126</sup>Y. Li, Z. Song, Y. Li, S. Chen, S. Li, Y. Li, H. Wang, and Z. Wang, *Sens. Actuators B Chem.* **282**, 259–267 (2019).
- <sup>127</sup>F. Liu, X. Chen, X. Wang, Y. Han, X. Song, J. Tian, X. He, and H. Cui, *Sens. Actuators B Chem.* **291**, 155–163 (2019).
- <sup>128</sup>H. Gao, Q. Yu, K. Chen, P. Sun, F. Liu, X. Yan, F. Liu, and G. Lu, *J. Colloid Interface Sci.* **535**, 458–468 (2019).
- <sup>129</sup>H. Yang, X. Bai, P. Hao, J. Tian, Y. Bo, X. Wang, and H. Liu, *Sens. Actuators B Chem.* **280**, 34–40 (2019).
- <sup>130</sup>F. Zhang, X. Dong, X. Cheng, Y. Xu, X. Zhang, and L. Huo, *ACS Appl. Mater. Interfaces* **11**, 11755–11762 (2019).
- <sup>131</sup>F. Qu, X. Zhou, B. Zhang, S. Zhang, C. Jiang, S. Ruan, and M. Yang, *J. Alloys Compd.* **782**, 672–678 (2019).
- <sup>132</sup>J. Li, H. Liu, H. Fu, L. Xu, H. Jin, X. Zhang, L. Wang, and K. Yu, *J. Alloys Compd.* **788**, 248–256 (2019).
- <sup>133</sup>Y. Li, X. Zhou, W. Luo, X. Cheng, Y. Zhu, A. M. El-Toni, A. Khan, Y. Deng, and D. Zhao, *Adv. Mater. Interfaces* **6**, 1801269 (2019).
- <sup>134</sup>V. K. Tomer, R. Malik, V. Chaudhary, A. Baruah, and L. Kienle, *Noble Metal-Metal Oxide Hybrid Nanoparticles* (Woodhead Publishing, 2019).
- <sup>135</sup>Y. Liang, W. Liu, W. Hu, Q. Zhou, K. He, K. Xu, Y. Yang, T. Yu, and C. Yuan, *Mater. Res. Bull.* **114**, 1–9 (2019).
- <sup>136</sup>G. Ren, Z. Li, W. Yang, M. Faheem, J. Xing, X. Zou, Q. Pan, G. Zhu, and Y. Du, *Sens. Actuators B Chem.* **284**, 421–427 (2019).
- <sup>137</sup>R. Yan, D. Gargas, and P. Yang, *Nat. Photonics* **3**, 569 (2009).
- <sup>138</sup>E. Comini and G. Sberveglieri, *Mater. Today* **13**, 36–44 (2010).
- <sup>139</sup>Y. Yong, H. Cui, Q. Zhou, X. Su, Y. Kuang, and X. Li, *J. Phys. Chem. Solids* **127**, 68–75 (2019).
- <sup>140</sup>J. H. Kim, A. Mirzaei, H. W. Kim, and S. S. Kim, *Sens. Actuators B: Chem.* **302**, 127150 (2020).
- <sup>141</sup>Q. Wan, Q. H. Li, Y. J. Chen, T. H. Wang, X. L. He, and J. P. Lin, *Appl. Phys. Lett.* **84**, 3654–3656 (2004).
- <sup>142</sup>F. Patolsky and C. M. Lieber, *Mater. Today* **8**, 20–28 (2005).
- <sup>143</sup>Z. L. Wang, *Nanowires and Nanobelts Materials, Properties and Devices. Volume 1: Metal and Semiconductor Nanowires* (Springer, New York, 2013).
- <sup>144</sup>R. S. Wagner and W. C. Ellis, *Appl. Phys. Lett.* **4**, 89–90 (1964).
- <sup>145</sup>D.-I. Suh, C. C. Byeon, and C.-L. Lee, *Appl. Surf. Sci.* **257**, 1454–1456 (2010).
- <sup>146</sup>S. V. Sivaram, H. Y. Hui, M. Mata, J. Arbiol, and M. A. Filler, *Nano Lett.* **16**, 6717–6723 (2016).
- <sup>147</sup>M. Ek and M. A. Filler, *Acc. Chem. Res.* **51**, 118–126 (2018).
- <sup>148</sup>S. Kim, J. H. Bang, M. S. Choi, W. Oum, A. Mirzaei, N. Lee, H.-C. Kwon, D. Lee, H. Jeon, S. S. Kim, and H. W. Kim, *Met. Mater. Int.* **25**, 805–813 (2019).
- <sup>149</sup>Y. Wu and P. Yang, *J. Am. Chem. Soc.* **123**, 3165–3166 (2001).
- <sup>150</sup>L. Yu, A. J. Riddle, S. Wang, A. Sundararajan, J. Thompson, Y.-J. Chang, M. E. Park, S. S. A. Seo, and B. S. Guiton, *Chem. Mater.* **28**, 8924–8929 (2016).
- <sup>151</sup>C. Cheng and H. J. Fan, *Nano Today* **7**, 327–343 (2012).
- <sup>152</sup>Q. Wan, J. Huang, Z. Xie, T. Wang, E. N. Dattoli, and W. Lu, *Appl. Phys. Lett.* **92**, 102101 (2008).
- <sup>153</sup>S. An, S. Park, H. Ko, C. Jin, W. I. Lee, and C. Lee, *Thin Solid Film* **547**, 241–245 (2013).
- <sup>154</sup>A. M. El-Toni, M. A. Habila, J. P. Labis, Z. A. AlOthman, M. Alhoshan, A. A. Elzatahry, and F. Zhang, *Nanoscale* **8**, 2510–2531 (2016).



- 155**P. Karnati, S. Akbar, and P. A. Morris, *Sens. Actuators B Chem.* **295**, 127–143 (2019).
- 156**R. G. Chaudhuri and S. Paria, *Chem. Rev.* **112**, 2373–2433 (2012).
- 157**D. Zappa, V. Galstyan, N. Kaur, H. M. M. Arachchige, O. Sisman, and E. Comini, *Anal. Chim. Acta* **1039**, 1–23 (2018).
- 158**J. Hämäläinen, M. Ritala, and M. Leskelä, *Chem. Mater.* **26**, 786–801 (2014).
- 159**M. Weber, E. Coy, I. Iatsunskyi, L. Yate, P. Miele, and M. Bechelany, *CrystEngComm* **19**, 6089–6094 (2017).
- 160**M. Weber, I. Iatsunskyi, E. Coy, P. Miele, D. Cornu, and M. Bechelany, *Adv. Mater. Interfaces* **5**(16), 1800056 (2018).
- 161**M. J. Weber, M. A. Verheijen, A. A. Bol, and W. M. M. Kessels, *Nanotechnology* **26**(9), 094002 (2015).
- 162**M. Leskelä and M. Ritala, *Thin Solid Films* **409**, 138–146 (2002).
- 163**S. M. George, *Chem. Rev.* **110**, 111–131 (2010).
- 164**C. Detavernier, J. Dendooven, S. P. Sree, K. F. Ludwig, and J. A. Martens, *Chem. Soc. Rev.* **40**, 5242–5253 (2011).
- 165**M. Weber, J.-Y. Kim, J.-H. Lee, J.-H. Kim, I. Iatsunskyi, E. Coy, P. Miele, M. Bechelany, and S. S. Kim, *J. Mater. Chem. A* **7**, 8107–8116 (2019).
- 166**L. Y. Zhu, K. Yuan, J. G. Yang, H. P. Ma, T. Wang, X. M. Ji, J. J. Feng, A. Devi, and H. L. Lu, *Sens. Actuators B: Chem.* **290**, 233–241 (2019).
- 167**L. Liao, H. B. Lu, J. C. Li, C. Liu, D. J. Fu, and Y. L. Liu, *Appl. Phys. Lett.* **91**, 173110 (2007).
- 168**L. Liao, H. X. Mai, Q. Yuan, H. B. Lu, J. C. Li, C. Liu, C. H. Yan, Z. X. Shen, and T. Yu, *J. Phys. Chem. C* **112**, 9061–9065 (2008).
- 169**A. Kolmakov, D. O. Klenov, Y. Lilach, S. Stemmer, and M. Moskovits, *Nano Lett.* **5**, 667–673 (2005).
- 170**M. Tonezzer and N. V. Hieu, *Sens. Actuators B Chem.* **163**, 146–152 (2012).
- 171**Y.-J. Choi, I.-S. Hwang, J.-G. Park, K. J. Choi, J.-H. Park, and J.-H. Lee, *Nanotechnology* **19**, 095508 (2008).
- 172**O. Lupan, V. V. Ursaki, G. Chai, L. Chow, G. A. Emelchenko, I. M. Tiginyanu, A. N. Gruzintsev, and A. N. Redkin, *Sens. Actuators B Chem.* **144**, 56–66 (2010).
- 173**M. Z. Asadzadeh, A. Köck, M. Popov, S. Steinhauer, J. Spitaler, and L. Rومانer, *Sens. Actuators B Chem.* **295**, 22–29 (2019).
- 174**D. Zhang, Z. Liu, C. Li, T. Tang, X. Liu, S. Han, B. Lei, and C. Zhou, *Nano Lett.* **4**, 1919–1924 (2004).
- 175**L. C. Tien, H. T. Wang, B. S. Kang, F. Ren, P. W. Sadik, D. P. Norton, S. J. Pearton, and J. Lin, *Electrochem. Solid-State Lett.* **8**, G230–G232 (2005).
- 176**J. H. Bang, M. S. Choi, A. Mirzaei, Y. J. Kwon, S. S. Kim, T. W. Kim, and H. W. Kim, *Sens. Actuators B Chem.* **274**, 356–369 (2018).
- 177**S. S. Kim, H. G. Na, S.-W. Choi, D. S. Kwak, and H. W. Kim, *J. Phys. D Appl. Phys.* **45**, 205301 (2012).
- 178**H. W. Kim, H. G. Na, Y. J. Kwon, H. Y. Cho, and C. Lee, *Sens. Actuators B Chem.* **219**, 22–29 (2015).
- 179**H.-S. Woo, C.-H. Kwak, J.-H. Chung, and J.-H. Lee, *ACS Appl. Mater. Interfaces* **6**, 22553–22560 (2014).
- 180**H.-S. Woo, C.-H. Kwak, J.-H. Chung, and J.-H. Lee, *Sens. Actuators B Chem.* **216**, 358–366 (2015).
- 181**J. Hubalek, J. Hradecky, V. Adam, O. Krystofova, D. Huska, M. Masarik, L. Trnkova, A. Horna, K. Klosova, M. Adamek, J. Zehnalek, and R. Kizek, *Sensors* **7**, 1238–1255 (2007).
- 182**U. Yogeswaran, S. Thiagarajan, and S.-M. Chen, *Anal. Biochem.* **365**, 122–131 (2007).
- 183**U. Yogeswaran and S.-M. Chen, *Sensors* **8**(1), 290–313 (2008).
- 184**M. H. Velez, *Thin Solid Films* **495**, 51–63 (2006).
- 185**O. Lupan, N. Wolff, V. Postica, T. Braniste, I. Paulowicz, V. Hrkac, Y. K. Mishra, I. Tiginyanu, L. Kienle, and R. Adelung, *Ceram. Int.* **44**(5), 4859–4867 (2018).
- 186**J. Kim, S.-D. Han, C. H. Han, J. Gwak, H. D. Lee, and J. S. Wang, *Sensors* **6**, 526–535 (2006).
- 187**M. Curreli, C. Li, Y. Sun, B. Lei, M. A. Gunderson, M. E. Thompson, and C. Zhou, *J. Am. Chem. Soc.* **127**, 6922–6923 (2005).
- 188**R. Laocharoensuk, A. Bulbarello, S. B. Hocevar, S. Mannino, B. Ogorevc, and J. Wang, *J. Am. Chem. Soc.* **129**, 7774–7775 (2007).
- 189**A. Hultgren, M. Tanase, E. J. Felton, K. Bhadriraju, A. K. Salem, C. S. Chen, and D. H. Reich, *Biotechnol. Prog.* **21**, 509–515 (2005).
- 190**M. B. Gawande, A. Goswami, T. Asefa, H. Guo, A. V. Biradar, D.-L. Peng, R. Zboril, and R. S. Varma, *Chem. Soc. Rev.* **44**, 7540–7590 (2015).
- 191**P. K. Kalambate, Dhanjai, Z. Huang, Y. Li, Y. Shen, M. Xie, Y. Huang, and A. K. Srivastava, “Core@shell nanomaterials based sensing devices: A review,” *Trends Anal. Chem.* **115**, 147–161 (2019).
- 192**J.-H. Kim, A. Katoch, and S. S. Kim, *Sens. Actuators B Chem.* **222**, 249–256 (2016).
- 193**J.-H. Kim, A. Katoch, S.-H. Kim, and S. S. Kim, *ACS Appl. Mater. Interfaces* **7**, 15351–15358 (2015).
- 194**S.-W. Choi, A. Katoch, G.-J. Sun, J.-H. Kim, S.-H. Kim, and S. S. Kim, *ACS Appl. Mater. Interfaces* **6**, 8281–8287 (2014).
- 195**X. Luo, X. Zheng, D. Wang, Y. Zhang, H. Cheng, X. Wang, H. Zhuang, and Y. Lou, *Sens. Actuators B: Chem.* **202**, 1010–1018 (2014).
- 196**Y. J. Kwon, H. G. Na, S. Y. Kang, M. S. Choi, J. H. Bang, T. W. Kim, A. Mirzaei, and H. W. Kim, *Sens. Actuators B Chem.* **239**, 180–192 (2017).
- 197**J. Rebholz, P. Bonanati, C. Jaeschke, M. M. L. Hübner, U. Weimar, and N. Barsan, *Sens. Actuators B Chem.* **188**, 631–636 (2013).
- 198**N. Hongsih, E. K. T. Wongrat, and S. Choopun, *Sens. Actuators B Chem.* **144**(1), 67–72 (2010).
- 199**J. X. Wang, X. W. Sun, Y. Yang, H. Huang, Y. C. Lee, O. K. Tan, and L. Vayssieres, *Nanotechnology* **17**(19), 4995–4998 (2006).
- 200**G. Korotcenkov, S. D. Han, B. K. Cho, and V. Brinzari, *Crit. Rev. Solid State Mater. Sci.* **34**(1–2), 1–17 (2009).
- 201**S. Park, H. Ko, S. Lee, H. Kim, and C. Lee, *Thin Solid Films* **570**, 298–302 (2014).
- 202**C. Jin, S. Park, H. Kim, and C. Lee, *Sens. Actuators B Chem.* **161**(1), 223–228 (2012).
- 203**A. Gurlo, N. Barsan, M. Ivanovskaya, U. Weimar, and W. Göpel, *Sens. Actuators B Chem.* **47**(1–3), 92–99 (1998).
- 204**Q. Xu, Z. Zhang, X. Song, S. Yuan, Z. Qiu, H. Xu, and B. Cao, *Sens. Actuators B Chem.* **245**, 375–385 (2017).
- 205**S. Seo, I. J. Park, M. Kim, S. Lee, C. Bae, H. S. Jung, N.-G. Park, J. Y. Kim, and H. Shin, *Nanoscale* **8**, 11403–11412 (2016).
- 206**Y. Yu, Y. Xia, W. Zeng, and R. Liu, *Mater. Lett.* **206**, 80–83 (2017).
- 207**C. Marichy, N. Donato, M. Latino, M. G. Willinger, J.-P. Tessonier, G. Neri, and N. Pinna, *Nanotechnology* **26**(1–7), 024004 (2015).
- 208**J.-H. Kim, A. Katoch, S.-W. Choi, and S. S. Kim, *Sens. Actuators B Chem.* **212**, 190–195 (2015).
- 209**H. Ko, S. Park, S. Lee, and C. Lee, *J. Nanosci. Nanotechnol.* **15**, 5295–5300 (2015).
- 210**M. S. Choi, A. Mirzaei, J. H. Bang, H. G. Na, C. Jin, S. S. Kim, and H. W. Kim, *J. Nanosci. Nanotechnol.* **19**, 6647–6655 (2019).
- 211**J.-H. Kim, A. Mirzaei, H. W. Kim, and S. S. Kim, *Sens. Actuators B Chem.* **285**, 358–367 (2019).
- 212**Z. U. Abideen, J.-H. Kim, A. Mirzaei, H. W. Kim, and S. S. Kim, *Sens. Actuators B Chem.* **255**, 1884–1896 (2018).
- 213**R. Leghrib, T. Dufour, F. Demoisson, N. Claessens, F. Reniers, and E. Llobet, *Sens. Actuators B Chem.* **160**, 974–980 (2011).
- 214**R. S. Ganesh, M. Navaneethan, V. L. Patil, S. Ponnusamy, C. Muthamizhchelvan, S. Kawasaki, P. S. Patil, and Y. Hayakawa, *Sens. Actuators B Chem.* **255**, 672–683 (2018).
- 215**J. Huang and Q. Wan, *Sensors* **9**, 9903–9924 (2009).
- 216**M. Tonezzer, J.-H. Kim, J.-H. Lee, S. Iannotta, and S. S. Kim, *Sens. Actuators B Chem.* **281**, 670–678 (2019).
- 217**J.-H. Kim, Y. Zheng, A. Mirzaei, and S. S. Kim, *Korean J. Mater. Res.* **26**, 741–750 (2016).
- 218**M. G. Chung, D.-H. Kim, D. K. Seo, T. Kim, H. U. Im, H. M. Lee, J.-B. Yoo, S.-H. Hong, T. J. Kang, and Y. H. Kim, *Sens. Actuators B Chem.* **169**, 387–392 (2012).

- 219**J. M. Walker, S. A. Akbar, and P. A. Morris, *Sens. Actuators B Chem.* **286**, 624–640 (2019).
- 220**K. Suematsu, K. Watanabe, A. Tou, Y. Sun, and K. Shimano, *Anal. Chem.* **90**, 1959–1966 (2018).
- 221**W. C. Conner, Jr., and J. L. Falconer, *Chem. Rev.* **95**, 759–788 (1995).
- 222**D.-T. Phan and G.-S. Chung, *Sens. Actuators B Chem.* **204**, 437–444 (2014).
- 223**Y. Luo, C. Zhang, B. Zheng, X. Geng, and M. Debliquy, *Int. J. Hydrogen Energy* **42**, 20386–20397 (2017).
- 224**A. V. Singhal, H. Charaya, and I. Lahiri, *Crit. Rev. Solid State* **42**, 499–526 (2017).
- 225**H.-J. Cho, V. T. Chen, S. Qiao, W.-T. Koo, R. M. Penner, and I.-D. Kim, *ACS Sens.* **3**, 2152–2158 (2018).
- 226**K. Nguyen, C. M. Hung, T. M. Ngoc, D. T. T. Le, D. H. Nguyen, D. Nguyen Van, and H. Nguyen Van, *Sens. Actuators B Chem.* **253**, 156–163 (2017).
- 227**X. Liu, J. Zhang, X. Guo, S. Wu, and S. Wang, *Sens. Actuators B Chem.* **152**(2), 162–167 (2011).
- 228**J. Chen, X. Yan, W. Liu, and Q. Xue, *Sens. Actuators B Chem.* **160**(1), 1499–1503 (2011).
- 229**G. Korotcenkov and B. K. Cho, *Sens. Actuators B Chem.* **198**, 316–341 (2014).
- 230**D. U. Hong, C.-H. Han, S. H. Park, I.-J. Kim, J. Gwak, S.-D. Han, and H. J. Kim, *Curr. Appl. Phys.* **9**(1), 172–178 (2009).
- 231**G. Korotcenkov and B. K. Cho, *Sens. Actuators B Chem.* **156**(2), 527–538 (2011).
- 232**D. R. Miller, S. A. Akbar, and P. A. Morris, *Sens. Actuators B Chem.* **204**, 250–272 (2014).
- 233**C. W. Na, H.-S. Woo, I.-D. Kim, and J.-H. Lee, *Chem. Commun.* **47**, 5148–5150 (2011).
- 234**P. Camagni, G. Faglia, P. Galinetto, C. Perego, G. Samoggia, and G. Sberveglieri, *Sens. Actuators B Chem.* **31**, 99–103 (1996).
- 235**M. Law, H. Kind, B. Messer, F. Kim, and P. Yang, *Angew. Chem. Int. Ed.* **41**, 2405–2408 (2002).
- 236**L. Zhu and W. Zeng, *Sens. Actuators A Phys.* **267**, 242–261 (2017).
- 237**E. Espid and F. Taghipour, *Crit. Rev. Solid State* **42**, 416–432 (2017).
- 238**S. Park, S. Kim, H. Ko, and C. Lee, *J. Electroceram.* **33**, 75–81 (2014).
- 239**Z. L. Wang, *Adv. Mater.* **24**, 280–285 (2012).
- 240**T. M. Ngoc, N. Van Duy, C. M. Hung, N. D. Hoa, H. Nguyen, M. Tonezzer, and N. Van Hieu, *Anal. Chim. Acta* **1069**, 108–116 (2019).
- 241**S. Xu, Y. Qin, C. Xu, Y. Wei, R. Yang, and Z. L. Wang, *Nat. Nanotechnol.* **5**, 366 (2010).
- 242**A. Salehi, *Sens. Actuators B Chem.* **96**, 88–93 (2003).
- 243**F. Yang, D. K. Taggart, and R. M. Small, *Small* **6**, 1422–1429 (2010).
- 244**C. S. Prajapati and N. Bhat, *Sens. Actuators B Chem.* **260**, 236–242 (2018).
- 245**J. D. Prades, R. Jimenez-Diaz, F. Hernandez-Ramirez, S. Barth, A. Cirera, A. Romano-Rodriguez, S. Mathur, and J. R. Morante, *Appl. Phys. Lett.* **93**, 123110 (2008).
- 246**C. Fàbrega, O. Casals, F. Hernández-Ramírez, and J. D. Prades, *Sens. Actuators B Chem.* **256**, 797–811 (2018).
- 247**T. F. Choo, N. U. Saidin, and K. Y. Kok, *Chem. Phys. Lett.* **713**, 180–184 (2018).
- 248**V. Demontis, M. Rocci, M. Donarelli, R. Maiti, V. Zannier, F. Beltram, L. Sorba, S. Roddaro, F. Rossella, and C. Baratto, *Sensors* **19**(13), 2994 (2019).
- 249**E. Comini, *Mater. Today* **19**, 559–567 (2016).
- 250**J.-H. Kim, H. W. Kim, and S. S. Kim, *Sens. Actuators B Chem.* **251**, 781–794 (2017).
- 251**J.-H. Kim, A. Mirzaei, H. W. Kim, and S. S. Kim, *Sens. Actuators B Chem.* **267**, 597–607 (2018).
- 252**R. Gutierrez-Osuna, *IEEE Sens. J.* **2**(3), 189–202 (2002).
- 253**S. Kiani, S. Minaei, and M. Ghasemi-Varnamkhashi, *J. Appl. Res. Med. Aromat. Plants* **3**(1), 1–9 (2016).
- 254**A. Loutfi, S. Coradeschi, G. K. Mani, P. Shankar, and J. B. B. Rayappan, *J. Food Eng.* **144**, 103–111 (2015).
- 255**K. Arshak, E. Moore, G. M. Lyons, J. Harris, and S. Clifford, *Sens. Rev.* **24**(2), 181–198 (2004).
- 256**J. Yan, X. Guo, S. Duan, P. Jia, L. Wang, C. Peng, and S. Zhang, *Sensors* **15**(11), 27804–27831 (2015).
- 257**A. D. Wilson, *Proc. Technol.* **1**, 453–463 (2012).
- 258**X. Chen, C. K. Y. Wong, C. A. Yuan, and G. Zhang, *Sens. Actuators B Chem.* **177**, 178–195 (2013).
- 259**J. M. Baik, M. Zielke, M. H. Kim, K. L. Turner, A. M. Wodtke, and M. Moskovits, *ACS Nano* **4**(6), 3117–3122 (2010).
- 260**V. V. Sysoev, B. K. Button, K. Wepsiec, S. Dmitriev, and A. Kolmakov, *Nano Lett.* **6**(8), 1584–1588 (2006).